Scientific report; 97 - 09

KNMI

On the assimilation of ozone into an atmospheric model

Elías Valur Hólm

De Bilt, 1997

Scientific report = wetenschappelijk rapport; WR 97 - 09

De Bilt, 1997

PO Box 201
3730 AE De Bilt
Wilhelminalaan 10
De Bilt
The Netherlands
Telephone + 31(0)30-220 69 11
Telefax + 31 (0)30-221 04 07

Author: Elías Valur Hólm*
*presently working at the ECMWF, Reading

UDC: 551.510.534
551.511.3
551.511.6

ISSN: 0169-1651

ISBN: 90-369-2132-5

EUMETSAT Fellowship Report: On the assimilation of ozone into an atmospheric model

Elías Valur Hólm

Abstract

A global shallow water model with a tracer transport equation is developed, and a theoretical demonstration is given of how dynamical information can be derived from tracer observations in this model using data assimilation. The advection scheme in the model is conservative and non-oscillatory and the model is second order accurate in time and space. An exact formal solution to the continuous and nonlinear data assimilation problem is given using the Euler-Lagrange equations, including both model errors and boundary conditions. The resulting system is a coupled boundary value problem in time. For illustration, the Euler-Lagrange equations are derived for the shallow water model. An appendix contains a tutorial on the solution of the Euler-Lagrange equations with the representer method.

Contents

Introduction

The work described in this report was performed as a EUMETSAT Research Fellowship 1995–1996 at the KNMI, The Netherlands. The goal of the Fellowship was to investigate the question *how dynamical information can be obtained from satellite ozone measurements for use in atmospheric models*. There are several conceivable ways to address this question, for example:

a) Theoretical and experimental study in a relevant *simplified model* of possible ways to derive dynamical information from ozone satellite measurements.
b) Computerized analysis of a series of satellite ozone images for deriving *ozone winds* in a manner similar to cloud wind retrievals.
c) Incorporation of ozone sensitive satellite radiance measurements in the *radiative transfer* models used in numerical weather prediction models.
d) Inclusion of ozone as a model variable in a weather prediction model and letting ozone measurements influence the dynamics of the model through the *data assimilation* system in use, just as any other measurements.

The above approaches are complementary, and at a numerical weather prediction center one would at one stage or another perform work along each of these lines. The last approach, the inclusion of ozone in a data assimilation system, must be considered as the ultimate step which puts satellite ozone measurements on equal footing with all other observations used in a weather prediction model. In a state of the art data assimilation system (Courtier et al. 1997) ozone winds, ozone sensitive radiances, retrieved total ozone and retrieved ozone profiles could all be treated in a consistent manner.

In the present study we will follow the first approach described above, and focus on the theoretical aspect of the problem in a simplified model. However, we will adress the question by formulating a very general data assimilation system for the simplified model, so that the concepts which we can adress will be much the same as in the last approach using a weather prediction model with state of the art data assimilation system. For understanding the basic concepts there is even an advantage to use a simplified system. Furthermore, when developing a new data assimilation system as in the present work, it is advisable to test the system on a simplified model version. The shallow water equations which will be used in the present work are recognized as an essential step on the way to full three dimensional weather prediction models, and is as such widely used for testing new concepts in numerical weather prediction.

The original plan for the present work is summarized in Fig. 0.1. The figure shows what has been achieved in the present work (thick) and what remains to be done (thin). The formulation and tests of the global shallow water model (SWE) with tracer is described in chapter 1. In chapter 2 a general theory for data assimilation with nonlinear models using the Euler–

Lagrange equations (EL) is summarised. In chapter 3 the theory is applied to the SWE model with a tracer, and it is seen how dynamical information can be obtained from tracer measurements. For the computational implementation of a data assimilation system based on the Euler–Lagrange equations, we use the concept of representers, and introduce the basic ideas in a simple way in an appendix. The actual programming of the data assimilation system has been performed, and preliminary experiments have been done, representing the last two parts of the work, which puts all other parts in their proper context. However, the results from the experiments show that work remains until the data assimilation system works properly. The further development and testing of the data assimilation system will be a part of future work.

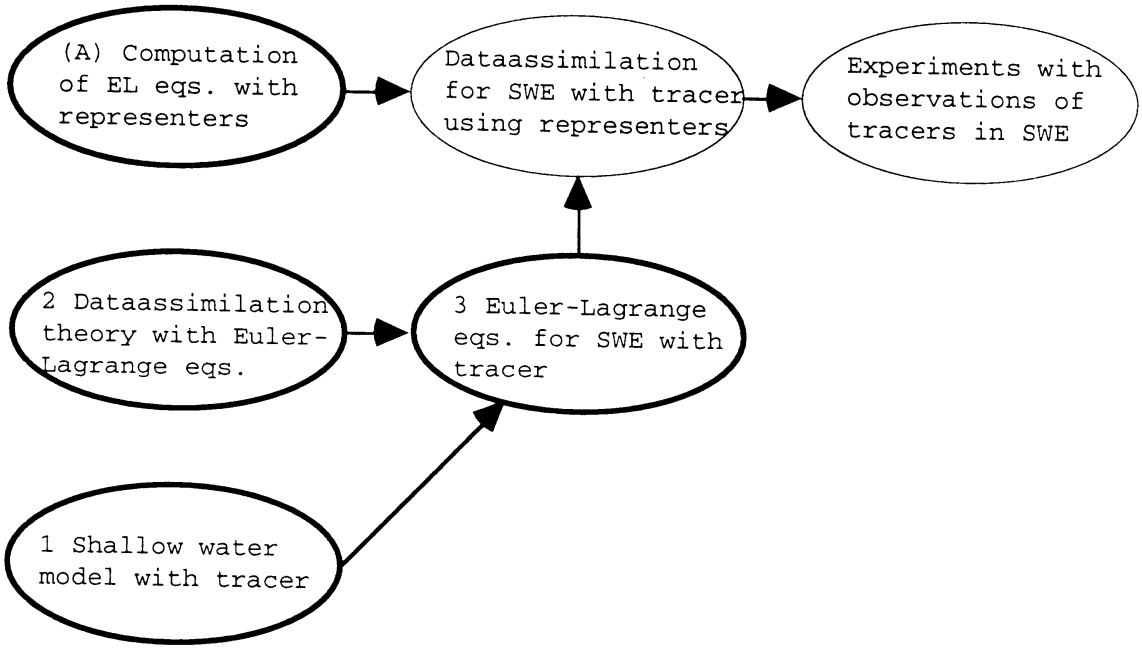

FIG. 0.1: Plan on how to derive meteorological information from tracer measurements (thick = work achieved during the EUMETSAT Fellowship; thin = remaining work). The columns represent the basic building blocks of the system (left column), the integration of different building blocks (middle column), and the tests of the integrated system (right column). The rows represent the basic dynamical model (bottom row), the data assimilation theory (middle row) and the computational implementation of the data assimilation system (top row).

Chapter 1

A global shallow water model with tracer transport

1.1 Introduction

The shallow water equations (SWE) are at the core of a description of atmospheric dynamics. The shallow water equations describe the time-evolution of the horizontal velocity and the height (or pressure) field of a fluid mass in which the whole column of the fluid moves together in the horizontal. The idea to use the two-dimensional SWE approximation is relevant for large scale motions in the atmosphere, which are mainly two-dimensional. There is also a strong link between the shallow water equations and three-dimensional atmospheric flow. The atmospheric flow can be approximated by a sum of several shallow water models, each multiplied by a vertical eigenfunction for the atmosphere, the Hough modes. Each of the shallow water models has an equivalent depth, ranging from circa 10 km and downwards. The atmospheric dynamics are then described by the evolution of all these SWE models interacting with each other.

An even simpler model for large scale atmospheric flow is the potential vorticity equation. But this model lacks some important features of the SWE model, such as divergence, gravity waves and adjustment processes of disturbances and instabilities from unbalanced to balanced states. Furthermore, the link with the three-dimensional atmospheric motion implicit in the shallow water equations is lacking in the potential vorticity model, which is basically an approximation of the two-dimensional large scale flow at divergence free levels in the atmosphere, which can be found at circa 500 hPa and 200 hPa.

Our aim is to address the question if and how satellite ozone measurements can be used to derive meteorological information. For this purpose we can use the shallow water equations, coupled with a two-dimensional tracer transport equation. Such a model can for example approximately describe the transport of total ozone. It has bee shown by Levelt et al. (1996) that total ozone transport can be approximated with single level winds at 200 hPa.

The shallow water and tracer transport model which we have developed is based on the advection schemes of Hólm (1995a, b) and a general curvilinear coordinate formulation of the shallow water equations given by Smolarkiewicz and Margolin (1993). The model is on finite volume form and conserves momentum and mass. The curvilinear coordinate formulation of the model makes it very flexible and useful for further development work.

We will begin with the description of the governing model equations in section 1.2, and turn to the numerical implementation of the system in section 1.3. Numerical tests of the dynamical evolution and the tracer transport are in section 1.4, followed by conclusions in section 1.5.

1.2 Formulation of the shallow water equations including a tracer

The formulation of the curvilinear model equations follow Smolarkiewicz and Margolin (1993). In the curvilinear coordinates the model equations have the same form everywhere, and can be discretized on a computational grid which has an even resolution in the computational space. In the curvilinear coordinate system the transformation from the Cartesian coordinate $\mathbf{x}'$ is built into the model variables and the differential operators. Thus all variables and operators are functions of the curvilinear coordinate $\mathbf{x} = (x, y)$, e. g. $\nabla = (\partial/\partial x, \partial/\partial y)$. The transformation to the curvilinear system is characterised by the Jacobian of the transformation, which is a product of the scale factors associated with the different coordinate directions, $G = G(\mathbf{x}) = h_x h_y$. The Jacobian measures how a unit volume in the curvilinear system expands and contracts relative a unit volume in the Cartesian system as a function of location, and the scale factors measure the linear expansion and contraction along different axis.

After introducing the Jacobian and the scale factors, the shallow water equations become

$$\frac{\partial GQ_x}{\partial t} + \nabla\cdot(\dot{\mathbf{x}}GQ_x) = -g\frac{G\Phi}{h_x}\frac{\partial}{\partial x}(\Phi + H_0) + [f + \frac{\dot{y}}{h_x}\frac{\partial h_y}{\partial x} - \frac{\dot{x}}{h_y}\frac{\partial h_x}{\partial y}]GQ_y \quad (1.1)$$

$$\frac{\partial GQ_y}{\partial t} + \nabla\cdot(\dot{\mathbf{x}}GQ_y) = -g\frac{G\Phi}{h_y}\frac{\partial}{\partial y}(\Phi + H_0) - [f + \frac{\dot{y}}{h_x}\frac{\partial h_y}{\partial x} - \frac{\dot{x}}{h_y}\frac{\partial h_x}{\partial y}]GQ_x \quad (1.2)$$

$$\frac{\partial G\Phi}{\partial t} + \nabla\cdot(\dot{\mathbf{x}}G\Phi) = 0 \quad (1.3)$$

$$\frac{\partial G\Psi}{\partial t} + \nabla\cdot(\dot{\mathbf{x}}G\Psi) = 0 \quad (1.4)$$

Here $\Phi(\mathbf{x}, t)$ is the thickness of the fluid and H_0 is the topography (see Fig. 1.1); the fluid momentum is $\mathbf{Q} = (Q_x, Q_y) = (\Phi\dot{x}h_x, \Phi\dot{y}h_y)$, $(\dot{x}, \dot{y})$ are velocities, and h_x and h_y are scale factors. In spherical coordinates $h_x = a\cos\theta$ and $h_y = a$, and $f = 2\Omega\sin\theta$, with a the radius, θ the latitude, and Ω the angular speed of rotation. Furthermore g is the gravitational acceleration. Finally Ψ is a passive tracer.

For more accurate numerical treatment, the model variable fluid thickness, Φ, is replaced by a perturbation Φ' around a mean surface level H_{00}. The new model variable is defined by the following relations

$$\Phi(\mathbf{x}, t) = \Phi_0(\mathbf{x}) + \Phi'(\mathbf{x}, t) \quad (1.5)$$

$$\Phi_0(\mathbf{x}) = H_{00} - H_0(\mathbf{x}) \quad (1.6)$$

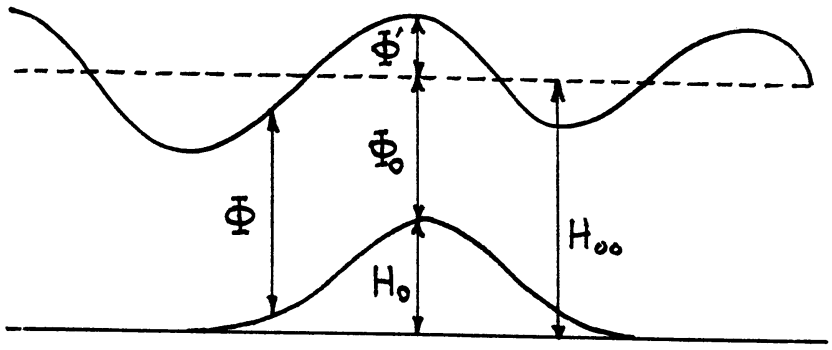

FIG. 1.1: The definition of a shallow water layer. H_0 is the topography, H_{00} is the mean surface level; Φ is the fluid thickness or "height"; Φ' is the "height perturbation".

With these definitions the pressure gradient term of Eqs. (1.1–1.2) becomes

$$G\Phi\,\nabla(H_0 + \Phi) = G\Phi\,\nabla(H_{00} + \Phi') = G\Phi\,\nabla\Phi' \tag{1.7}$$

and the divergence term in Eq. (1.3) becomes

$$\nabla\cdot(\dot{\mathbf{x}}G\Phi) = \nabla\cdot(\dot{\mathbf{x}}G\Phi') + \nabla\cdot(\dot{\mathbf{x}}G\Phi_0) \tag{1.8}$$

Insertion of Eqs. (1.7–1.8) in Eqs. (1.1–1.3) now gives

$$\frac{\partial GQ_x}{\partial t} + \nabla\cdot(\dot{\mathbf{x}}GQ_x) = -g\frac{(G\Phi_0 + G\Phi')}{h_x}\frac{\partial\Phi'}{\partial x} + [f + \frac{\dot{y}}{h_x}\frac{\partial h_y}{\partial x} - \frac{\dot{x}}{h_y}\frac{\partial h_x}{\partial y}]GQ_y \tag{1.9}$$

$$\frac{\partial GQ_y}{\partial t} + \nabla\cdot(\dot{\mathbf{x}}GQ_y) = -g\frac{(G\Phi_0 + G\Phi')}{h_y}\frac{\partial\Phi'}{\partial y} - [f + \frac{\dot{y}}{h_x}\frac{\partial h_y}{\partial x} - \frac{\dot{x}}{h_y}\frac{\partial h_x}{\partial y}]GQ_x \tag{1.10}$$

$$\frac{\partial G\Phi'}{\partial t} + \nabla\cdot(\dot{\mathbf{x}}G\Phi') = -\nabla\cdot(\dot{\mathbf{x}}G\Phi_0) \tag{1.11}$$

By defining a model vector $\mathbf{q}$, the shallow water equations with tracer can be written on the following compact form (with *subscript t* for partial time-derivative and *superscript t* for vector transpose)

$$\mathbf{q} = (q_1, q_2, q_3, q_4)^t = (GQ_x, GQ_y, G\Phi', G\Psi)^t \tag{1.12}$$

$$\mathbf{q}_t + \nabla\cdot(\dot{\mathbf{x}}\mathbf{q}) = \mathbf{F}(\mathbf{q}) \tag{1.13}$$

1.3 Numerical integration technique

The time integration of the shallow water equations uses explicit finite volume technique, consisting of an advection scheme and evaluation of the

forcing terms. For the advection of all variables (momentum, height and tracer) the most efficient of the high-order non-oscillatory algorithms with forward-in-time differencing described in Hólm (1995a, b), FCM2, is used. The solution advances from timelevel n to $n+1$ with a timestep Δt, employing the fully second order time-accurate correction of the forward-in-time algorithm given by Smolarkiewicz and Margolin (1993). The numerical integration algorithm can then be written as

$$\mathbf{q}^{n+1/2} = \boldsymbol{A}(\mathbf{q}^n, \dot{\mathbf{x}}^n, \frac{\Delta t}{2}) + \frac{\Delta t}{2}\mathbf{F}^n \tag{1.14}$$

$$\dot{\mathbf{x}}^{n+1/2} = \dot{\mathbf{x}}(\mathbf{q}^{n+1/2}) \tag{1.15}$$

$$\mathbf{q}^{n+1} = \boldsymbol{A}(\mathbf{q}^n + \frac{\Delta t}{2}\mathbf{F}^n, \dot{\mathbf{x}}^{n+1/2}, \Delta t) + \frac{\Delta t}{2}\mathbf{F}^{n+1} \tag{1.16}$$

In the above equations the operator $\boldsymbol{A}$ denotes the advection scheme, so that in e. g. Eq. (1.16), an advection step with length Δt is performed with the fluxes calculated from $\mathbf{q}^n + \frac{\Delta t}{2}\mathbf{F}^n$ and advective velocity $\dot{\mathbf{x}}^{n+1/2}$. The first step of the algorithm, Eqs. (1.14–1.15), give the advective velocity $\dot{\mathbf{x}}^{n+1/2}$ which is needed in the advection of Eq. (1.16). The advantage of using the nonlinear velocity extrapolation of Eqs. (1.14–1.15) is that the resulting velocities are consistent with the model equations, and allow four times longer timestep compared with a linear extrapolation, according to the experiments of Smolarkiewicz and Margolin (1993). The second step, Eq. (1.16), performs the advection and adds half the forcing calculated at the end of the timestep. This is the essence of the second order time accuracy of the algorithm, that the applied forcing is an average of the forcing at the begin and the end of the timestep. Since the forcing is a function of the solution itself, it is calculated iteratively after the advection has been performed. Experimentation showed that two iterations were enough, and further iterations did not improve the solution (see Smolarkiewicz and Margolin 1993 for a detailed discussion of the forcing calculation).

1.4 Advection tests

We will test the shallow water model on three different situations. The first two are standard tests (Williamson et al. 1992): a steady state nonlinear zonal geostrophic flow and a Rossby-Haurwitz wave. The last test shows the models response to the inclusion of topography. In the tests we will also look at the tracer transported by the shallow water model.

1.4.1 Steady state nonlinear zonal geostrophic flow

This first test has analytical solutions for both the shallow water equations (steady state) and the transported tracer (solid body rotation). By varying the angle between the poles of the computational grid and the Earth´s rotation

axis, the sensitivity of the model to the computational grid can be tested. This test is particularly useful for detecting problems at the poles of the computational grid, where the grid transformation factors vary rapidly.

The initial condition for this test (Williamson et al. 1992) is a zonal flow, but with the feature that the computational grid can be rotated by an angle $\alpha\pi$ relative the rotation axis of the Earth. This enables a simulation of for example cross-polar flow by rotating the computational grid 0.5π. The analytic solution of zonal flow on the rotated computational grid is

$$u(\lambda, \phi) = u_0 (\cos\theta \cos\alpha + \sin\lambda \sin\theta \sin\alpha) \tag{1.17}$$

$$v(\lambda, \phi) = -u_0 \sin\lambda \sin\alpha \tag{1.18}$$

$$\Phi(\lambda, \phi) = H_{00} - g^{-1} (a\Omega u_0 + \frac{1}{2}u_0^2)(-\cos\lambda \cos\theta \sin\alpha + \sin\theta \cos\alpha)^2 \tag{1.19}$$

and the corresponding Coriolis parameter is

$$f(\lambda, \phi) = 2\Omega(-\cos\lambda \cos\theta \sin\alpha + \sin\theta \cos\alpha) \tag{1.20}$$

Here $a = 6.37122 \times 10^6$ m, $\Omega = 7.292 \times 10^{-5}$ s^{-1} and $g = 9.80616$ m s^{-2}. In the test below we will simulate cross polar flow ($\alpha = 0.5$), with $H_{00} = 3000$ m, and $u_0 = 2\pi a/(12 \text{ days}) \approx 38.61$ m s^{-1}. The model is integrated for 12 days (8640 timesteps), which is the period of the solid body rotation, with a timestep of 120 s. This very short time-step comes from the accumulation of computational points near the poles. The model resolution is 128 points in longitude and 64 points in latitude.

Figure 1.2 compares the velocity and height perturbation at initial time (analytical solution) and after 12 days of integration. The two solutions are almost indistinguishable. In Fig. 1.3 the error growth of the solution is shown. The error in the wind is ca. 0.1 m/s (~1 %) and in the height perturbation ca. 1 m (~0.1 %) after 12 days.

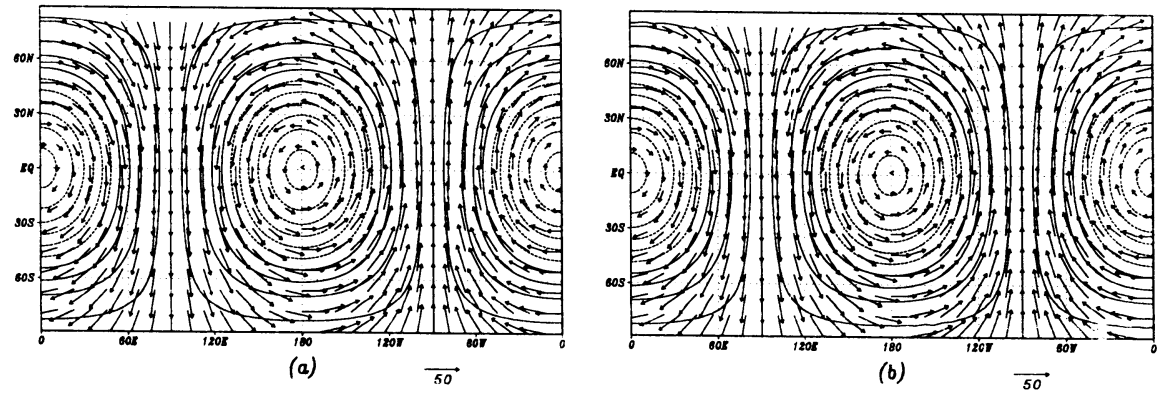

FIG. 1.2: Cross–polar flow. (a) Initial velocity and height perturbation. (b) Velocity and height perturbation at day 12. The reference wind arrow is 50 m/s long, and the height isoline interval is 200 m, with negative isolines dashed.

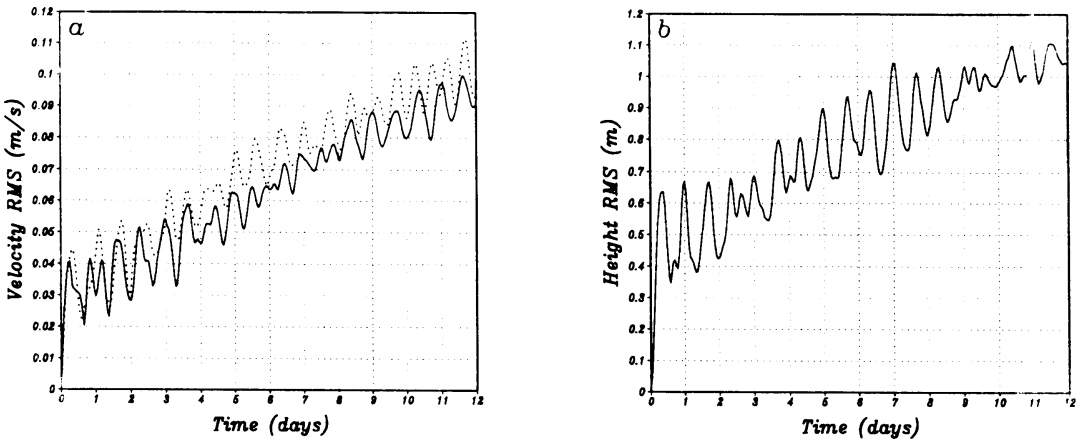

FIG. 1.3: RMS error for cross-polar flow. (a) Velocity (zonal velocity solid, meridional velocity dotted). (b) Perturbation height. The RMS error is an area weighted global average.

In the present steady state flow across the poles, the tracer distribution should be rotated without changing form. For the tracer we have chosen a realistic total ozone distribution obtained from the ECMWF model. There is a lot of small scale variation in this field which gives a stringent test of the advection scheme.

Figure 1.4 shows the tracer distribution at the initial time and after 12 days (one rotation). Note that the advecting velocity is taken from the model at each timestep, which is a more demanding test than just using a constant wind field. The tracer distribution has diffused somewhat, but all features are in the right place. There is very little distortion visible associated with the passage across the poles.

In Fig. 1.5 we look at longitudinal and latitudinal cross sections of the tracer distribution at day 12 and compare it with the analytical solution. The differences which we see are mainly due to diffusion at the extreme values of the field. No noise is visible in the numerical solution.

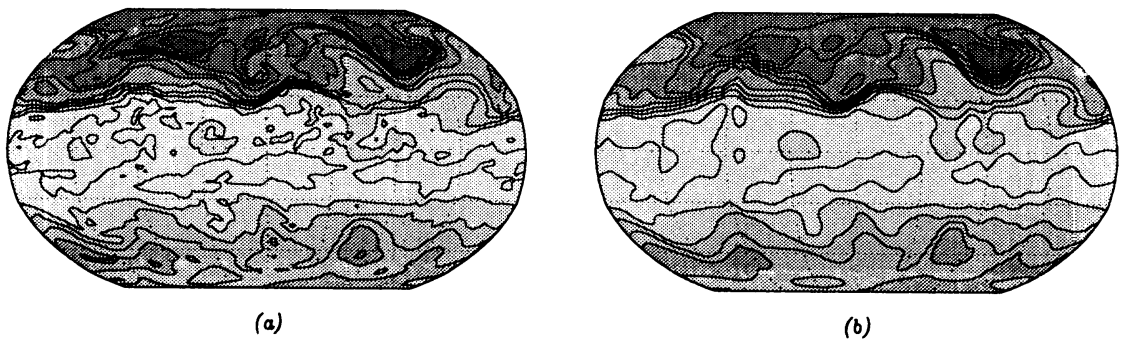

FIG. 1.4: Tracer (ozone) distribution in cross-polar flow. (a) Initial field, taken from ECMWF model total ozone. (b) Tracer after one rotation at day 12. The isoline interval is 25 Dobson units and higher values are darker.

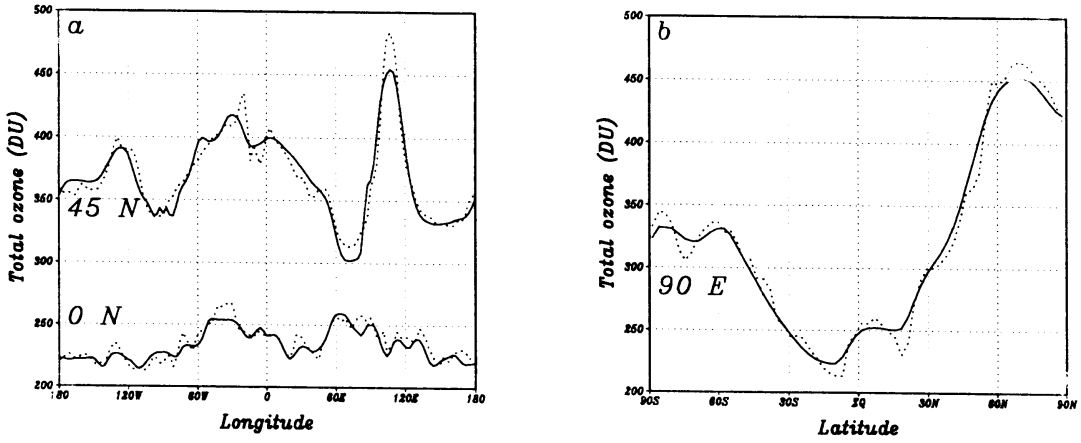

FIG. 1.5: Tracer (ozone) cross sections at day 12, one rotation (solid lines) compared with the analytical solution (dotted). (a) Longitudinal cross sections at ca. 0N and ca. 45N. (b) Latitudinal cross section at 90E, where the tracer has crossed the poles.

1.4.2 Rossby–Haurwitz wave

The Rossby–Haurwitz waves are not analytical solutions to the shallow-water equations on the sphere, but are standard tests more demanding than the steady state test above. The initial conditions are given by Williamson et al. (1992),

$$u(\lambda, \phi) = a\omega \cos\theta + aK \cos^{R-1}\theta \,(R \sin^2\theta - \cos^2\theta) \cos R\lambda \tag{1.21}$$

$$v(\lambda, \phi) = -aK \cos^{R-1}\theta \;\sin\theta \sin R\lambda \tag{1.22}$$

$$\begin{aligned}\Phi(\lambda, \phi) = H_{00} + \frac{a^2}{g}\{ &\frac{\omega}{2}(2\Omega+\omega)\cos^2\theta + \frac{K^2}{4}\cos^{2R-2}\theta\,[(R+1)\cos^4\theta + (2R^2-R-2)\cos^2\theta - 2R^2] \\ &+ \cos R\lambda \,\frac{2(\Omega+\omega)K}{(R+1)(R+2)}\cos^R\theta\,[(R^2+2R+2) - (R+1)^2\cos^2\theta] \\ &+ \cos 2R\lambda \,\frac{K^2}{4}\cos^{2R}\theta\,[(R+1)\cos^2\theta - (R+2)]\}\end{aligned} \tag{1.23}$$

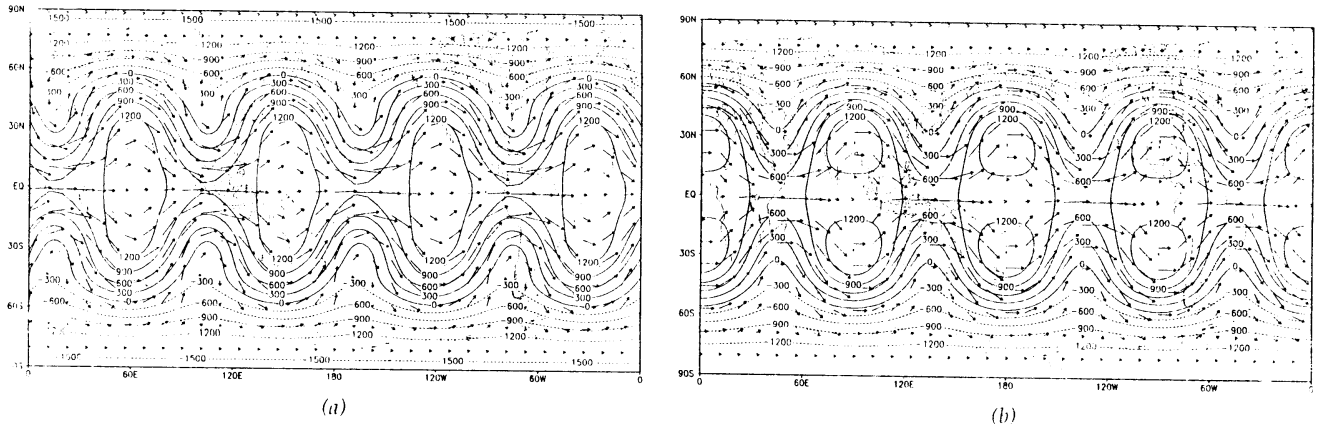

FIG. 1.6: Rossby-Haurwitz wave velocity and height perturbation fields. (a) Initial fields. (b) Fields after 14 days of integration.

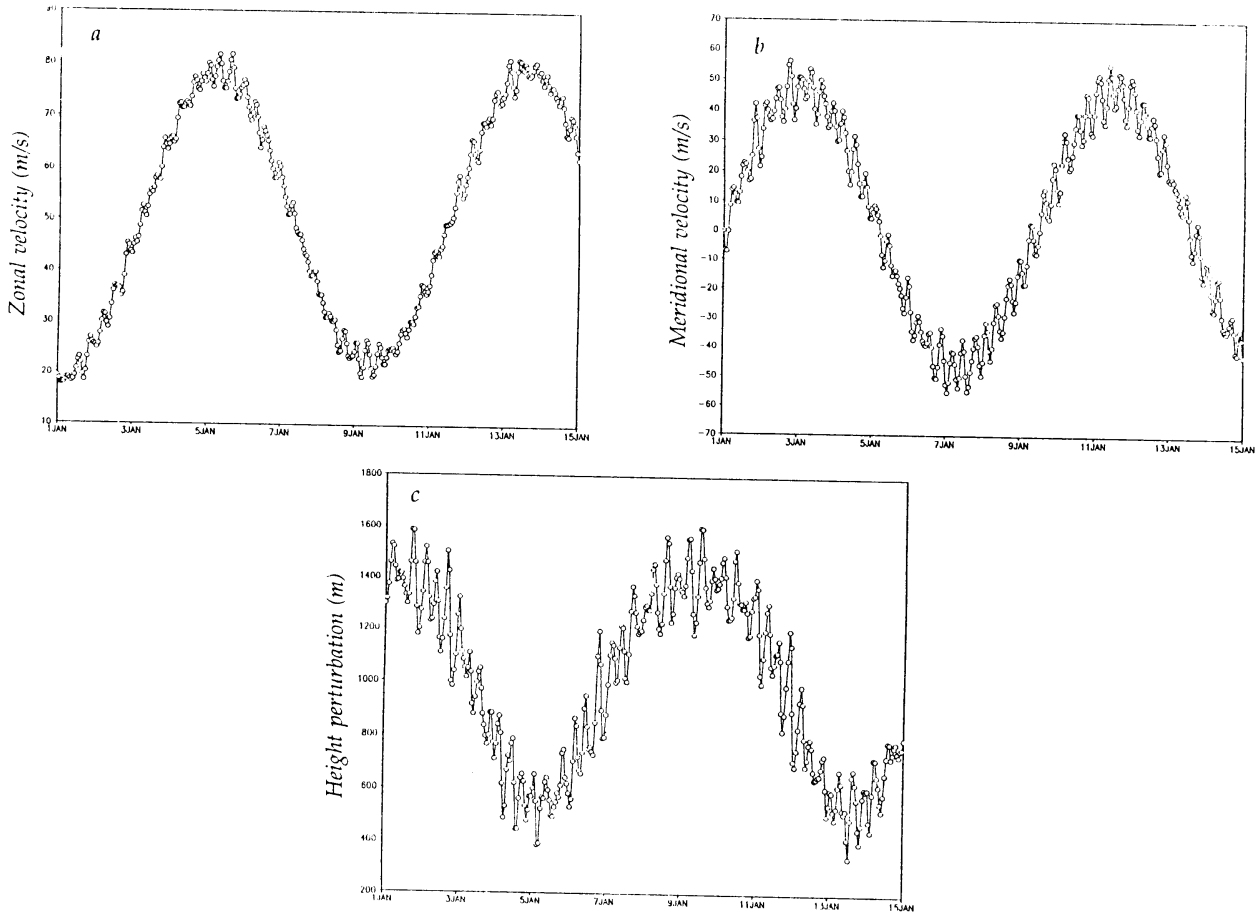

FIG. 1.7: Rossby-Haurwitz wave, time evolution at a single gridpoint (15.45N, 0E). (a) Zonal velocity. (b) Meridional velocity. (c) Height perturbation.

Here the parameters chosen are $\omega = K = 7.848 \times 10^{-6}$ s^{-1}, $H_{00} = 8 \times 10^3$ m and the wave number $R = 4$. The model resolution is 128 points in longitude and 64 points in latitude, and the timestep is 120 s as above, and the model is integrated for 14 days (10080 timesteps).

The velocity field and height perturbation at the beginning and end of the simulation are shown in Fig. 1.6. The solution changes form slightly during the simulation, due to that the phase speed decreases with latitude. This change is expected for the divergent equations used here, although a quantitative comparison with an accurate reference solution is necessary to complete the evaluation of the phase speed accuracy.

Figure 1.7 shows hourly outputs of the model at one gridpoint (15.45 N, 0 E). We see a periodic motion with a high-frequency inertial wave and a low-frequency Rossby wave. We see that the amplitude of the flow is conserved. This shows that there is very little diffusion in the present model, considering that there have been over 10000 timesteps. This good behaviour of the model comes back in the total energy of the flow which fluctuates with an amplitude of ca 0.3 % around the initial value, without any systematic increase or decrease of total energy.

1.4.3 Flow with topography

In the last test of the model, we investigate how the model performs with topography included. Since there are no analytical solutions, we will concentrate on the qualitative features of the flow, as well as on the total energy conservation.

The topography H_0 is averaged onto the model grid from the 0.25° by 0.25° US Navy topography. The model resolution and timestep is the same as above (128 by 64 gridpoints, 120 s timestep). As an initial condition we take a zonal flow similar to Eqs. (1.17–19), except that we replace the fluid thickness in the lhs of Eq. (1.19) with fluid thickness plus topography. Then the fluid surface is identical to the surface of the steady state solution, with a constant elevation along each longitude. We have $u(\lambda, \phi, 0) = u_0 \cos\theta$, $v(\lambda, \phi, 0) = 0$, and $\Phi(\lambda, \phi, 0) = -H_0(\lambda, \phi) + H_{00} - g^{-1}(a\Omega u_0 + \frac{1}{2}u_0^2)\sin^2\theta$, with the parameters $H_{00} = 8000$ m, and $u_0 = 30$ m/s. The model is integrated for 12 days.

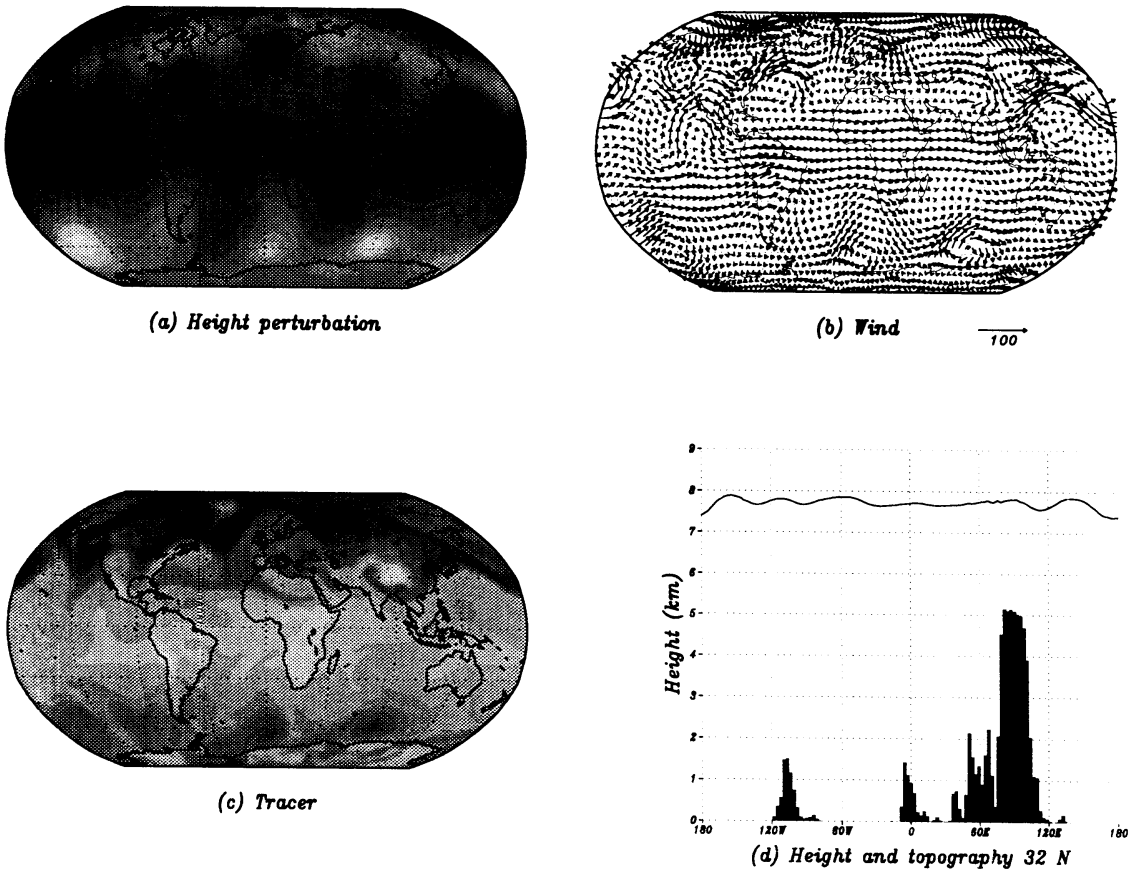

FIG. 1.8: Flow over topography at day 12. (a) Height perturbation field. (b) Wind field (c) Tracer field. (d) Cross-section of height field and topography over Himalaya, 32N. In the height and tracer figures higher values are darker.

Figure 1.8 shows the model integration results at day 12. The tracer distribution, which initially is uncorrelated with the flow (see Fig. 4a)

develops flow consistent features. The tracer concentrations become higher in atmospheric lows (note the four lows at 60S), and become lower in atmospheric highs and over topography (e. g. over Himalaya and east of North America). The dynamics evolve smoothly from the zonal initial conditions, and there are no visible problems in the wind field or in the height field. The inclusion of topography causes no problems, as we can see when looking at the total height field in Fig. 8d.

The total energy, which should be conserved in a nondissipative system, decreases very slowly with time. At the end of the 12 day simulation 99.93 % of the initial energy remains, which is very good. The good energy conservation can be attributed to the fully second order accurate treatment of the equations following Smolarkiewicz and Margolin (1993), as shown by Hólm (1996a) in the context of incompressible flow.

1.5 Conclusions

We have shown the first test results from a global shallow water model with a tracer. The results show that the model gives an accurate solution of the SWE system, with low dispersion and low diffusion. The model has no problems to resolve cross polar flow, or flow over topography, which can be attributed to the general curvilinear coordinate formulation of the model. In particular it has been shown that the model is non-oscillatory, which guarantees that no artificial maxima or minima appear. This last point is most visible in the solid body tracer advection tests. Since the model is formulated on finite volume form, it is per definition mass and momentum conserving, and the tracer amount is conserved aswell. The total energy of the model is very well conserved, although this was no design feature of the model.

In summary, although the present model is quite accurate, further development is needed to achieve a practical timestep length. The main limitation on the timestep length appears at the poles of the latitudinal-longitudinal grid used in the computation, and further developments of the model should concentrate on removing this limitation. This will be done by reducing the model resolution near the poles.

Chapter 2

Nonlinear continuous formulation of variational data assimilation using the Euler–Lagrange equations: a constructive approach

2.1 Introduction

Data assimilation deals with the general problem of how to describe a physical system by way of combining physical models and observed data. The practical solution to this problem is to device fast and accurate algorithms for the discrete problem at hand. Examples of efficient data assimilation algorithms in meteorology include optimum interpolation and variational data assimilation. Several different theoretical descriptions have been used as a foundation for data assimilation, based for example on control theory, information theory, probability theory, and variational analysis (see Daley 1991, Tarantola 1987, and Menke 1984 for further references). One use of a theoretical approach is to suggest which simplifications to make to achieve fast and accurate data assimilation algorithms. The result is often similar, with different theoretical approaches leading to equivalent algorithms. However, the theory is also a tool in itself for a deeper understanding of the physical system (Tarantola and Valette 1982, Bennett 1992). In particular, if a theoretical description is possible without the assumptions necessary for an efficient algorithm, this is preferable, since then a particular algorithm becomes a special case, and different algorithms can be related to each other (Lorenc 1986, Courtier 1997).

In most applications of data assimilation in meteorology the physical models are nonlinear and the observation data depend nonlinearly on the physical system. Most, if not all, efficient data assimilation algorithms depend on some linearization techniques applied to a discretized version of the nonlinear problem. However, this practical aspect must not be allowed to obscure that it is straightforward to derive continuous equations for the full nonlinear problem. For example, variational analysis applied to the data assimilation problem gives the full nonlinear solution in terms of the Euler–Lagrange equations (Bennett 1992).

Here we will derive the Euler–Lagrange equations that solve the data assimilation for nonlinear models and data with given boundary conditions. We will derive formulations using the standard L_2 norm (minimisation of squared errors). The material presented in this chapter is mostly from Bennett (1992), although the presentation and notations differ.

2.2 Model and data

The most general description of the nonlinear model would be just a single nonlinear model operator $\mathbf{M}(\mathbf{q})$. However, we are aiming at a constructive

data assimilation approach for time dependent fluid dynamical models. For these fluid dynamical models it is natural to treat the time dimension separately, since the only time-derivative terms involved are the tendencies of the model variables themselves. Separating the time tendencies from the remainder of the model operator will make the resulting Euler–Lagrange equations easier to understand. Below we will follow this approach.

We consider a nonlinear physical model and observation data given on the region V with a boundary S. The length of the timeperiod over which observations and model are adjusted to each other is T. Then

$$\mathbf{q}_t = \mathbf{F}^0(\mathbf{q}) + \mathbf{F}'(\mathbf{x}, t) \tag{2.1}$$

$$\mathbf{q}(\mathbf{x}, 0) = \mathbf{q}^0(\mathbf{x}, 0) + \mathbf{q}'(\mathbf{x}, 0) \tag{2.2}$$

$$\mathbf{G}(\mathbf{q}) = \mathbf{g}^0(\mathbf{s}, t) + \mathbf{g}'(\mathbf{s}, t), \quad \mathbf{s} \in S \tag{2.3}$$

$$\mathbf{E}(\mathbf{q}) = \mathbf{e}^0(\mathbf{x}, t) + \mathbf{e}'(\mathbf{x}, t) \tag{2.4}$$

$$d_m = H_m(\mathbf{q}) + d'_m, \quad m = 1, 2, \ldots, M \tag{2.5}$$

Here $\mathbf{q}$ is a vector of variables describing the true state of the physical system. The time evolution of $\mathbf{q}$ is given by the known nonlinear forcing $\mathbf{F}^0$ and the model error $\mathbf{F}'$.

The initial condition is given by the prior estimate of the state $\mathbf{q}^0$, and the error in the prior estimate $\mathbf{q}'$.

The boundary conditions are expressed by the boundary condition operator $\mathbf{G}$ being equal to a boundary forcing. The prior estimate of the boundary forcing is $\mathbf{g}^0$, with error $\mathbf{g}'$. As an example, at a solid boundary the normal velocity vanishes, so the velocity component of $\mathbf{G}$ is a derivative normal to the boundary, and the corresponding components of $\mathbf{g}^0$ and $\mathbf{g}'$ are zero. Another example is when the velocity is given from a global model on the boundary of a limited area model. The velocity components in $\mathbf{G}$, $\mathbf{g}^0$, and $\mathbf{g}'$ are then the identity operator, the global model velocity, and the error in the global model velocity, respectively.

All additional constraints on the physical system are described by the operator $\mathbf{E}$. This operator is constrained by $\mathbf{e}^0$ within the error $\mathbf{e}'$, which defines how well the constraint should be fulfilled ($\mathbf{e}' = 0$ for an exact constraint). Examples of such constraints are dynamical and/or chemical balances which the system is known to be close to, or which the system must fulfil exactly. If for example a certain smoothness is required of the solution, $\mathbf{E}$ could be a diffusion operator.

The M observation data d_m are related to the physical system through the nonlinear observation operators H_m. The observation error is d'_m. Generally, the observation data are obtained as weighted averages in time and space. The location of an observation in time and space is defined by multiplying the observation equation, Eq. (2.5), with a weighting function

$\phi_m(\mathbf{x}, t)$ with the following property

$$\int_V d\mathbf{x} \int_0^T dt\, \phi_m(\mathbf{x}, t) = 1 \tag{2.6}$$

In other words, we divide the observation operator into a location independent part, and a weight function that defines the location of the observation. For example, a Dirac delta function in time and space can be used in Eq. (2.6) to identify an observation with a given location at a given instant and box functions can be used to describe an average in time and space. For an aeroplane observation a sausage formed weight function along the flight path could be used. For a satellite observation, a column stretching from satellite to surface could be appropriate. For convenience, the observations in Eq. (2.5) multiplied by Eq. (2.6) are summarised in the vectors **H**, **d**, and **d**′,

$$\int_V d\mathbf{x} \int_0^T dt\, \phi_m(\mathbf{x}, t)\, d_m = \int_V d\mathbf{x} \int_0^T dt\, \phi_m(\mathbf{x}, t)\, [H_m(\mathbf{q}) + d'_m] \tag{2.7a}$$

$$\mathbf{d}(\mathbf{x}, t) = \mathbf{H}(\mathbf{q}) + \mathbf{d}'(\mathbf{x}, t) \tag{2.7b}$$

The prior estimate $\mathbf{q}^0(\mathbf{x}, t)$ is obtained by integrating the model using only the known forcing and the prior initial conditions and boundary forcing. The boundary condition operator **G** usually involves a combination of the variables **q** and their derivatives normal to the boundary. The prior boundary forcing for the region of interest is usually obtained from lower resolution model integrations covering a much larger region. The vector of observation operators **H** includes all steps needed to go from the physical variables **q** to the observation data **d**, including for example radiative transfer models, interpolations, and averaging in time and/or space.

2.3 Formulation of a variational problem to fit model and data

The problem at hand can be stated as follows:

> *Derive as accurate description as possible of a physical system from a given physical model, prior initial and boundary conditions, constraints, and observation data, all of which are approximate.*

To complete the theoretical description of the problem, a norm has to be chosen to measure the accuracy of the description. To actually solve the problem, the weights of each term of the approximate description must first be determined from statistics of the errors in model, initial conditions, boundary conditions, constraints and observation data. An essential point is that the statistics imply an underlying probability distribution of the errors. For each different probability distribution there is a corresponding norm

that best measures the accuracy (Menke 1984, Lorenc 1986, Tarantola 1987). When the error statistics differ from the probability distribution implied by the chosen norm, the optimal solution can be completely unreasonable. The almost universally applied norm is L_2, which implies a Gaussian probability distribution for the errors. The popularity of the L_2 norm is based on its ease of application and the efficiency of the resulting algorithms. However, a weakness of all algorithms based on the L_2 norm is their sensitivity: one isolated outlier in the data can completely change the solution (Tarantola 1987, Menke 1984). The L_2 norm algorithms thus fail when the error probability distribution differs much from the Gaussian distribution. Similar arguments apply to other norms. However, algorithms based on the L_1 norm (implying exponential error distribution) are particularly robust against outliers in data (Tarantola 1987, Menke 1984). The drawbacks of the L_1 norm methods are their complexity and inefficiency as compared with the L_2 norm methods, in particular for large models.

After these words of caution, we will now formulate the variational data assimilation problem using the L_2 norm.

Let the optimum solution be one which minimises the sum of the errors in model, constraints, boundary conditions, initial conditions, and observation data, measured by the L_2 norm,

$$\begin{aligned} J_2[\mathbf{q}] = & \int_V d\mathbf{x} \int_0^T dt \int_V d\mathbf{x}' \int_0^T dt'\, \mathbf{F}'^{t}(\mathbf{x}, t)\, \mathbf{W}_f(\mathbf{x}, t, \mathbf{x}', t')\mathbf{F}'(\mathbf{x}', t') \\ & + \int_V d\mathbf{x} \int_0^T dt \int_V d\mathbf{x}' \int_0^T dt'\, \mathbf{e}'^{t}(\mathbf{x}, t)\, \mathbf{W}_e(\mathbf{x}, t, \mathbf{x}', t')\mathbf{e}'(\mathbf{x}', t') \\ & + \oint_S d\mathbf{s} \int_0^T dt \oint_S d\mathbf{s}' \int_0^T dt'\, \mathbf{g}'^{t}(\mathbf{s}, t)\, \mathbf{W}_g(\mathbf{s}, t, \mathbf{s}', t')\mathbf{g}'(\mathbf{s}', t') \\ & + \int_V d\mathbf{x} \int_V d\mathbf{x}'\, \mathbf{q}'^{t}(\mathbf{x}, 0)\mathbf{W}_i(\mathbf{x}, \mathbf{x}')\mathbf{q}'(\mathbf{x}', 0) + \mathbf{d}'^{t}\mathbf{W}_d\,\mathbf{d}' \end{aligned} \tag{2.8}$$

This expression is also called a cost function. We prefer to write out all integrals in full, since it makes it easier to follow the details of the derivation. Here $\mathbf{W}_f$, $\mathbf{W}_g$, $\mathbf{W}_e$, $\mathbf{W}_i$, and $\mathbf{W}_d$ are weight matrices associated with the error in model, boundary conditions, constraints, initial conditions and observation data, respectively[1]. These weights are the inverses of the corresponding covariance matrices, which are all positive definite and symmetric. In the above formulation, cross correlations between model, initial conditions, boundary conditions, constraints, and measurements respectively, are assumed zero. Insertion of Eqs. (2.1–2.7) in Eq. (2.8) gives

---

[1]Note that Roman vectors are written $\mathbf{d}$, etc., but since the printer does not print bold Greek letters, Greek vectors are written with overbar, $\bar{\eta}$, etc. Matrices are written as $\mathbf{W}_d$ etc., and transposes as $\mathbf{d}^t$, etc. Functionals are written as J, etc.

$$
\begin{aligned}
J_2[\mathbf{q}] = &\int_V d\mathbf{x} \int_0^T dt \int_V d\mathbf{x}' \int_0^T dt' \, [\mathbf{q}_t - \mathbf{F}^0(\mathbf{q})]^t \, \mathbf{W}_f \, [\mathbf{q}_t - \mathbf{F}^0(\mathbf{q})]' \\
&+ \int_V d\mathbf{x} \int_0^T dt \int_V d\mathbf{x}' \int_0^T dt' \, [\mathbf{E}(\mathbf{q}) - \mathbf{e}^0]^t \, \mathbf{W}_e \, [\mathbf{E}(\mathbf{q}) - \mathbf{e}^0]' \\
&+ \oint_S d\mathbf{s} \int_0^T dt \oint_S d\mathbf{s}' \int_0^T dt' \, [\mathbf{G}(\mathbf{q}) - \mathbf{g}^0]^t \, \mathbf{W}_g \, [\mathbf{G}(\mathbf{q}) - \mathbf{g}^0]' \\
&+ \int_V d\mathbf{x} \int_V d\mathbf{x}' \, [\mathbf{q} - \mathbf{q}^0]^t \, \mathbf{W}_i \, [\mathbf{q} - \mathbf{q}^0]' + [\mathbf{d} - \mathbf{H}(\mathbf{q})]^t \, \mathbf{W}_d \, [\mathbf{d} - \mathbf{H}(\mathbf{q})]'
\end{aligned}
\tag{2.9}
$$

Here primed square brackets, [ ]′, are used as a shorthand for evaluating a function in the primed coordinates $(\mathbf{x}', t')$. Now the standard tools of variational analysis can be used to obtain the optimum solution (see e. g. Goldstein 1980, chapter 2). Let $\hat{\mathbf{q}}$ be an optimum solution which gives the minimum of $J_2[\mathbf{q}]$ with respect to a variation of $\mathbf{q}$. Define

$$
\mathbf{q}(\mathbf{x}, t) = \hat{\mathbf{q}}(\mathbf{x}, t) + \gamma \bar{\eta}(\mathbf{x}, t) \tag{2.10}
$$

where γ is a constant and $\bar{\eta}(\mathbf{x}, t)$ is an arbitrary vector function (with dependent components however). The minimum of Eq. (2.9) is found from

$$
\frac{dJ_2}{d\gamma} \Big|_{\gamma = 0} = 0 \tag{2.11}
$$

2.4 General solution of the L_2 norm variational problem

Inserting Eq. (2.10) in Eq. (2.9) gives (note that all weight matrices are positive definite and symmetric)

$$
\begin{aligned}
J_2[\mathbf{q}] = &\int_V d\mathbf{x} \int_0^T dt \int_V d\mathbf{x}' \int_0^T dt' \, [\hat{\mathbf{q}}_t + \gamma\bar{\eta}_t - \mathbf{F}^0(\hat{\mathbf{q}} + \gamma\bar{\eta})]^t \, \mathbf{W}_f \, [\hat{\mathbf{q}}_t + \gamma\bar{\eta}_t - \mathbf{F}^0(\hat{\mathbf{q}} + \gamma\bar{\eta})]' \\
&+ \int_V d\mathbf{x} \int_0^T dt \int_V d\mathbf{x}' \int_0^T dt' \, [\mathbf{E}(\hat{\mathbf{q}} + \gamma\bar{\eta}) - \mathbf{e}^0]^t \, \mathbf{W}_e \, [\mathbf{E}(\hat{\mathbf{q}} + \gamma\bar{\eta}) - \mathbf{e}^0]' \\
&+ \oint_S d\mathbf{s} \int_0^T dt \oint_S d\mathbf{s}' \int_0^T dt' \, [\mathbf{G}(\hat{\mathbf{q}} + \gamma\bar{\eta}) - \mathbf{g}^0]^t \, \mathbf{W}_g \, [\mathbf{G}(\hat{\mathbf{q}} + \gamma\bar{\eta}) - \mathbf{g}^0]' \\
&+ \int_V d\mathbf{x} \int_V d\mathbf{x}' \, [\hat{\mathbf{q}} + \gamma\bar{\eta} - \mathbf{q}^0]^t \, \mathbf{W}_i \, [\hat{\mathbf{q}} + \gamma\bar{\eta} - \mathbf{q}^0]' \\
&+ [\mathbf{d} - \mathbf{H}(\hat{\mathbf{q}} + \gamma\bar{\eta})]^t \, \mathbf{W}_d \, [\mathbf{d} - \mathbf{H}(\hat{\mathbf{q}} + \gamma\bar{\eta})]'
\end{aligned}
\tag{2.12}
$$

Before we differentiate the cost function, let us note a rule for the

differentiation of the involved operators by the following example,

$$\frac{d\mathbf{F}^0(\hat{\mathbf{q}}+\gamma\bar{\eta})}{d\gamma}\Big|_{\gamma=0} = \frac{\partial \mathbf{F}^0(\mathbf{q})}{\partial \mathbf{q}}\Big|_{\mathbf{q}=\hat{\mathbf{q}}}\bar{\eta} \tag{2.13}$$

Furthermore, introduce a simplified notation for the functional derivative,

$$\frac{\partial \mathbf{F}^0}{\partial \hat{\mathbf{q}}} = \frac{\partial \mathbf{F}^0(\mathbf{q})}{\partial \mathbf{q}}\Big|_{\mathbf{q}=\hat{\mathbf{q}}} \tag{2.14}$$

Equations (2.13–14) of course also apply to the operators $\mathbf{E}$, $\mathbf{G}$ and $\mathbf{H}$. Differentiation of the cost function now gives

$$\begin{aligned}\frac{1}{2}\frac{dJ_2}{d\gamma}\Big|_{\gamma=0} = &\int_V dx \int_0^T dt \int_V dx' \int_0^T dt' \left[\bar{\eta}_t - \frac{\partial \mathbf{F}^0}{\partial \hat{\mathbf{q}}}\bar{\eta}\right]^t \mathbf{W}_f \left[\hat{\mathbf{q}}_t - \mathbf{F}^0(\hat{\mathbf{q}})\right]' \\ &+ \int_V dx \int_0^T dt \int_V dx' \int_0^T dt' \left[\frac{\partial \mathbf{E}}{\partial \hat{\mathbf{q}}}\bar{\eta}\right]^t \mathbf{W}_e \left[\mathbf{E}(\hat{\mathbf{q}}) - \mathbf{e}^0\right]' \\ &+ \oint_S ds \int_0^T dt \oint_S ds' \int_0^T dt' \left[\frac{\partial \mathbf{G}}{\partial \hat{\mathbf{q}}}\bar{\eta}\right]^t \mathbf{W}_g \left[\mathbf{G}(\hat{\mathbf{q}}) - \mathbf{g}^0\right]' \\ &+ \int_V dx \int_V dx' \, \bar{\eta}^t \mathbf{W}_i \left[\hat{\mathbf{q}} - \mathbf{q}^0\right]' - \left[\frac{\partial \mathbf{H}}{\partial \hat{\mathbf{q}}}\bar{\eta}\right]^t \mathbf{W}_d \left[\mathbf{d} - \mathbf{H}(\hat{\mathbf{q}})\right]'\end{aligned} \tag{2.15}$$

We see that the terms in this equation are products of operators acting on the arbitrary function $\bar{\eta}$ and expressions involving the optimum state $\hat{\mathbf{q}}$. *Note that the operators are linear in* $\bar{\eta}$ *even if they are nonlinear in* $\hat{\mathbf{q}}$. If we can rearrange the above equation so that $\bar{\eta}$ only appears as a multiplicative factor, then the remaining expressions must be zero at the minimum of the functional according to Eq. (2.11), which will give the sought equations for the optimum state. This can be achieved by partial integrations with respect to $\mathbf{x}$ and t after introducing the vector variables $\bar{\lambda}$, $\bar{\omega}$, $\bar{\mu}$, and $\bar{\nu}$,

$$\bar{\lambda}(\mathbf{x}, t) = \int_V dx' \int_0^T dt' \, \mathbf{W}_f(\mathbf{x}, t, \mathbf{x}', t') \left[\hat{\mathbf{q}}_t - \mathbf{F}^0(\hat{\mathbf{q}})\right]' \tag{2.16}$$

$$\bar{\omega}(\mathbf{x}, t) = \int_V dx' \int_0^T dt' \, \mathbf{W}_e(\mathbf{x}, t, \mathbf{x}', t') \left[\mathbf{E}(\hat{\mathbf{q}}) - \mathbf{e}^0\right]' \tag{2.17}$$

$$\bar{\mu}(\mathbf{s}, t) = \oint_S ds' \int_0^T dt' \, \mathbf{W}_g(\mathbf{s}, t, \mathbf{s}', t') \left[\mathbf{G}(\hat{\mathbf{q}}) - \mathbf{g}^0\right]' \tag{2.18}$$

$$\bar{\nu} = \mathbf{W}_d \left[\mathbf{d} - \mathbf{H}(\hat{\mathbf{q}})\right]' \tag{2.19}$$

Inserting the above definitions in Eq. (2.15) and using Eq. (2.11) then gives

$$\frac{1}{2}\frac{dJ_2}{d\gamma}\Big|_{\gamma=0} = 0 = \int_V dx \int_0^T dt\,[\bar{\eta}_t - \frac{\partial F^0}{\partial \hat{q}}\bar{\eta}]^t \bar{\lambda} + \int_V dx \int_0^T dt\,[\frac{\partial E}{\partial \hat{q}}\bar{\eta}]^t \bar{\omega} - [\frac{\partial H}{\partial \hat{q}}\bar{\eta}]^t \bar{\nu}$$
$$+ \oint_S ds \int_0^T dt\,[\frac{\partial G}{\partial \hat{q}}\bar{\eta}]^t \bar{\mu} + \int_V dx \int_V dx'\,\bar{\eta}^t \mathbf{W}_i\,[\hat{q} - q^0]' \qquad (2.20)$$

2.4.1 The definition and construction of adjoint operators

The functional in Eq. (2.20), the gradient of the cost function, is linear in the arbitrary vector function $\bar{\eta}$. *Thus the gradient of the cost function is a linear functional, although the model and data are nonlinear.* By repeated partial integrations it is always possible to move all derivatives of $\bar{\eta}$ to derivatives of the functions $\bar{\lambda}$, $\bar{\mu}$, $\bar{\omega}$, and $\bar{\nu}$. In the process of partial integration, boundary terms appear which have to be accounted for (here we mean boundaries in the general sense, including the time direction). As an example, the first term on the right hand side of Eq. (2.20) becomes

$$\int_V dx \int_0^T dt\,[\frac{\partial \bar{\eta}}{\partial t}]^t \bar{\lambda} = \int_V dx\,[\bar{\eta}^t(x, t)\bar{\lambda}(x, t)]_{t=0}^{t=T} - \int_V dx \int_0^T dt\,\bar{\eta}^t \frac{\partial \bar{\lambda}}{\partial t} \qquad (2.21)$$

Using Dirac delta functions to express the boundary terms, we can write this equation as

$$\int_V dx \int_0^T dt\,[\frac{\partial \bar{\eta}}{\partial t}]^t \bar{\lambda} = = \int_V dx \int_0^T dt \left[[\delta(t - T) - \delta(t) - \frac{\partial}{\partial t}]\bar{\lambda}\right]^t \bar{\eta} \qquad (2.22)$$

A shorthand notion for this process of partial integration is offered by the concept of adjoint operators from the theory of linear operators (see e. g. Kolmogorov and Fomin, 1957). The adjoint operator A^* of the operator A is defined by

$$\langle Af, g\rangle = \langle f, A^* g\rangle \qquad (2.23)$$

where $\langle \cdot, \cdot \rangle$ is a suitable scalar product. *It is worth noting that in finite-dimensional space linear operators are given by matrices, and the adjoint A^* is given by the transpose of the matrix for the operator A.*

Now take Eq. (2.22) as an illustration of the concepts involved in the definition of the adjoint operator. By inspection A and the adjoint A^* are seen to be

$$A = \frac{\partial}{\partial t} \Rightarrow A^* = \delta(t - T) - \delta(t) - \frac{\partial}{\partial t} \qquad (2.24)$$

We thus see that if a linear operator includes timederivatives, the adjoint operator has additional terms at the initial and end times of the integration.

Generally, if a linear operator has any derivatives normal to a boundary, additional boundary terms appear in the adjoint operator.

As an illustration, consider a transformation of the coordinates **x** and t to boundary following coordinates $\bar{\xi}$, where time is one of the coordinates. The boundary is then composed of isosurfaces of the coordinates ξ_i. The linear operator now includes mixed and/or unmixed derivatives. Unmixed derivatives in the variable ξ_i will give additional terms in the adjoint operator on the boundary surfaces where ξ_i is constant. Mixed derivatives in ξ_i and ξ_j will give additional terms to the adjoint on the intersection of the corresponding boundary planes, and so on.

An alternative notation for the adjoint that summarises the above discussion will now be given. In the present case, where we treat the time and space dimension separately, we can divide the adjoint operator into four parts defined in the interior of our domain, on its spatial boundary, and at initial and end times,

$$A^* = A^*_V + A^*_S + A^*_0 + A^*_T \tag{2.25}$$

Generally, the division of an adjoint operator into parts follows naturally from the construction of the adjoint by partial integrations, and the division can be performed in any way as to fit the particular problem. For example, a further subdivision of the boundary terms to fit a particular problem is possible, as in Bennett (1992), where the terms for inflow, outflow, and solid boundaries are treated separately.

2.4.2 The adjoint equations

By repeated partial integrations the adjoint of any linear operator can be constructed and written on the form of Eq. (2.25). We will now in turn treat each of the terms of the gradient of the cost function, which is a linear functional in $\bar{\eta}$.

The time derivative term has been solved by Eq. (2.21). The model forcing term is given by

$$-\int_V dx \int_0^T dt \left[\frac{\partial \mathbf{F}^0}{\partial \hat{\mathbf{q}}} \bar{\eta}\right]^t \bar{\lambda} = -\int_V dx \int_0^T dt\, \bar{\eta}^t \left(\frac{\partial \mathbf{F}^0}{\partial \hat{\mathbf{q}}}\right)^*_V \bar{\lambda} - \oint_S ds \int_0^T dt\, \bar{\eta}^t \left(\frac{\partial \mathbf{F}^0}{\partial \hat{\mathbf{q}}}\right)^*_S \bar{\lambda} \tag{2.26}$$

Note that $\mathbf{F}^0$ usually contains spatial derivatives, so that the derivation of the adjoints is not trivial (this applies for the adjoints below aswell). The constraint term, including possible spatial and temporal derivatives, is on the form

$$\begin{aligned}\int_V dx \int_0^T dt \left[\frac{\partial \mathbf{E}}{\partial \hat{\mathbf{q}}} \bar{\eta}\right]^t \bar{\omega} = &\int_V dx \int_0^T dt\, \bar{\eta}^t \left(\frac{\partial \mathbf{E}}{\partial \hat{\mathbf{q}}}\right)^*_V \bar{\omega} + \oint_S ds \int_0^T dt\, \bar{\eta}^t \left(\frac{\partial \mathbf{E}}{\partial \hat{\mathbf{q}}}\right)^*_S \bar{\omega} \\ &- \int_V dx\, \bar{\eta}^t \left(\frac{\partial \mathbf{E}}{\partial \hat{\mathbf{q}}}\right)^*_0 \bar{\omega} + \int_V dx\, \bar{\eta}^t \left(\frac{\partial \mathbf{E}}{\partial \hat{\mathbf{q}}}\right)^*_T \bar{\omega}\end{aligned} \tag{2.27}$$

The boundary term does at most include derivatives normal to the boundary,

$$\oint_S ds \int_0^T dt \left[\frac{\partial \mathbf{G}}{\partial \hat{\mathbf{q}}} \bar{\eta}\right]^t \bar{\mu} = \oint_S ds \int_0^T dt\, \bar{\eta}^t \left(\frac{\partial \mathbf{G}}{\partial \hat{\mathbf{q}}}\right)_S^* \bar{\mu} \tag{2.28}$$

The observation operator can generally include spatial and temporal derivatives, but an observation will only contribute to the initial, end or boundary conditions when the weighting function that defines the location of the observation is nonzero there, $\phi_m(\mathbf{x}, t) \neq 0$. First, insert the definition of the weight function, Eq. (2.6),

$$-\left[\frac{\partial \mathbf{H}}{\partial \hat{\mathbf{q}}} \bar{\eta}\right]^t \bar{\nu} = -\int_V dx \int_0^T dt \sum_{m=1}^{M} \phi_m \left[\frac{\partial H_m}{\partial \hat{\mathbf{q}}} \bar{\eta}\right] \nu_m \tag{2.29}$$

Then we get

$$\begin{aligned} -\int_V dx \int_0^T dt\, \phi_m \left[\frac{\partial H_m}{\partial \hat{\mathbf{q}}} \bar{\eta}\right] \nu_m = &-\int_V dx\, \bar{\eta}^t \left(\frac{\partial H_m}{\partial \hat{\mathbf{q}}}\right)_0^* (\phi_m \nu_m) - \int_V dx\, \bar{\eta}^t \left(\frac{\partial H_m}{\partial \hat{\mathbf{q}}}\right)_T^* (\phi_m \nu_m) \\ &- \int_V dx \int_0^T dt\, \bar{\eta}^t \left(\frac{\partial H_m}{\partial \hat{\mathbf{q}}}\right)_V^* (\phi_m \nu_m) - \oint_S ds \int_0^T dt\, \bar{\eta}^t \left(\frac{\partial H_m}{\partial \hat{\mathbf{q}}}\right)_S^* (\phi_m \nu_m) \end{aligned} \tag{2.30}$$

Now all terms can be collected together and inserted in Eq. (2.20),

$$\begin{aligned} \frac{1}{2}\frac{dJ_2}{d\gamma}\Big|_{\gamma=0} = 0 = &\int_V dx \int_0^T dt\, \bar{\eta}^t(\mathbf{x}, t) \left[-\frac{\partial \bar{\lambda}}{\partial t} - \left(\frac{\partial \mathbf{F}^0}{\partial \hat{\mathbf{q}}}\right)_V^* \bar{\lambda} + \left(\frac{\partial \mathbf{E}}{\partial \hat{\mathbf{q}}}\right)_V^* \bar{\omega} - \sum_{m=1}^{M} \left(\frac{\partial H_m}{\partial \hat{\mathbf{q}}}\right)_V^* (\phi_m \nu_m)\right] \\ &+ \oint_S ds \int_0^T dt\, \bar{\eta}^t(\mathbf{s}, t) \left[\left(\frac{\partial \mathbf{G}}{\partial \hat{\mathbf{q}}}\right)_S^* \bar{\mu} - \left(\frac{\partial \mathbf{F}^0}{\partial \hat{\mathbf{q}}}\right)_S^* \bar{\lambda} + \left(\frac{\partial \mathbf{E}}{\partial \hat{\mathbf{q}}}\right)_S^* \bar{\omega} - \sum_{m=1}^{M} \left(\frac{\partial H_m}{\partial \hat{\mathbf{q}}}\right)_S^* (\phi_m \nu_m)\right] \\ &+ \int_V dx\, \bar{\eta}^t(\mathbf{x}, 0) \left[\int_V dx'\, \mathbf{W}_i [\hat{\mathbf{q}} - \mathbf{q}^0]' - \bar{\lambda} + \left(\frac{\partial \mathbf{E}}{\partial \hat{\mathbf{q}}}\right)_0^* \bar{\omega} - \sum_{m=1}^{M} \left(\frac{\partial H_m}{\partial \hat{\mathbf{q}}}\right)_0^* (\phi_m \nu_m)\right] \\ &+ \int_V dx\, \bar{\eta}^t(\mathbf{x}, T) \left[\bar{\lambda} + \left(\frac{\partial \mathbf{E}}{\partial \hat{\mathbf{q}}}\right)_T^* \bar{\omega} - \sum_{m=1}^{M} \left(\frac{\partial H_m}{\partial \hat{\mathbf{q}}}\right)_T^* (\phi_m \nu_m)\right] \end{aligned} \tag{2.31}$$

The final equations now follow from that the arbitrary vector function $\bar{\eta}$ can be varied independently in each of the four integrals in the above equation, for example by changing $\bar{\eta}$ on the boundary only, etc. Therefore the only way for Eq. (2.31) to be fulfilled is that each of the expressions following $\bar{\eta}$ in the four integrals are identically zero. This gives

$$\bar{\lambda}(\mathbf{x}, T) = -\left(\frac{\partial \mathbf{E}}{\partial \hat{\mathbf{q}}}\right)_T^* \bar{\omega}(\mathbf{x}, T) + \sum_{m=1}^{M} \left(\frac{\partial H_m}{\partial \hat{\mathbf{q}}}\right)_T^* [\phi_m(\mathbf{x}, T) \nu_m] \tag{2.32}$$

$$-\frac{\partial \bar{\lambda}(\mathbf{x}, t)}{\partial t} = \left(\frac{\partial \mathbf{F}^0}{\partial \hat{\mathbf{q}}}\right)^*_V \bar{\lambda}(\mathbf{x}, t) - \left(\frac{\partial \mathbf{E}}{\partial \hat{\mathbf{q}}}\right)^*_V \bar{\omega}(\mathbf{x}, t) + \sum_{m=1}^{M} \left(\frac{\partial H_m}{\partial \hat{\mathbf{q}}}\right)^*_V [\phi_m(\mathbf{x}, t) v_m] \quad (2.33)$$

$$-\left(\frac{\partial \mathbf{F}^0}{\partial \hat{\mathbf{q}}}\right)^*_S \bar{\lambda}(\mathbf{s}, t) = -\left(\frac{\partial \mathbf{G}}{\partial \hat{\mathbf{q}}}\right)^*_S \bar{\mu}(\mathbf{s}, t) - \left(\frac{\partial \mathbf{E}}{\partial \hat{\mathbf{q}}}\right)^*_S \bar{\omega}(\mathbf{s}, t) + \sum_{m=1}^{M} \left(\frac{\partial H_m}{\partial \hat{\mathbf{q}}}\right)^*_S [\phi_m(\mathbf{s}, t) v_m] \quad (2.34)$$

$$\mathbf{q}'(\mathbf{x}, 0) = \int_V d\mathbf{x}' \mathbf{W}_i^{-1}(\mathbf{x}, \mathbf{x}')\{\bar{\lambda}(\mathbf{x}', 0) - \left(\frac{\partial \mathbf{E}}{\partial \hat{\mathbf{q}}}\right)^*_0 \bar{\omega}(\mathbf{x}', 0) + \sum_{m=1}^{M} \left(\frac{\partial H_m}{\partial \hat{\mathbf{q}}}\right)^*_0 [\phi_m(\mathbf{x}', 0) v_m]\} \quad (2.35)$$

Equations (2.32–34) are now the Euler–Lagrange equation for the system, with end and boundary conditions, and Eq. (2.35) is the initial condition for the forward equation. Note that $\bar{\mu}$, $\bar{\omega}$, and $\bar{\nu}$ are functions of the optimal state $\hat{\mathbf{q}}$ according to their definition in Eqs. (2.17–2.19). Thus the solution of the Euler–Lagrange equations needs the solution of the forward equations as input. We will return to the consequences this has on a computational implementation in the summary of the solution in section 2.5

2.4.3 Optimal corrections to the forward equations

We now use the definitions of $\bar{\mu}$, $\bar{\omega}$, and $\bar{\nu}$, Eqs. (2.16–2.19), together with Eq. (2.31) to obtain the optimal estimates of the errors in boundary condition, constraints, and model forcing,

$$\mathbf{F}'(\mathbf{x}, t) = \int_V d\mathbf{x}' \int_0^T dt' \mathbf{W}_f^{-1}(\mathbf{x}, t, \mathbf{x}', t') \bar{\lambda}(\mathbf{x}', t') \quad (2.36)$$

$$\mathbf{e}'(\mathbf{x}, t) = \int_V d\mathbf{x}' \int_0^T dt' \mathbf{W}_e^{-1}(\mathbf{x}, t, \mathbf{x}', t') \bar{\omega}(\mathbf{x}', t') \quad (2.37)$$

$$\mathbf{g}'(\mathbf{s}, t) = \oint_S d\mathbf{s}' \int_0^T dt' \mathbf{W}_g^{-1}(\mathbf{s}, t, \mathbf{s}', t') \bar{\mu}(\mathbf{s}', t') \quad (2.38)$$

We see that the optimal corrections to the forward equations need the solution of the Euler–Lagrange (or adjoint) equations. These formulas are obtained by inserting the following definitions of the inverse error weight matrices (Bennett, 1992)

$$\int_V d\mathbf{x}\, \mathbf{W}_i^{-1}(\mathbf{x}'', \mathbf{x}) \mathbf{W}_i(\mathbf{x}, \mathbf{x}') = \delta(\mathbf{x}'' - \mathbf{x}')\, \mathbf{I} \quad (2.39)$$

$$\int_V d\mathbf{x} \int_0^T dt\, \mathbf{W}_f^{-1}(\mathbf{x}'', t'', \mathbf{x}, t) \mathbf{W}_f(\mathbf{x}, t, \mathbf{x}', t') = \delta(\mathbf{x}'' - \mathbf{x}')\delta(t'' - t')\, \mathbf{I} \quad (2.40)$$

$$\int_V dx \int_0^T dt\, \mathbf{W}_e^{-1}(x'', t'', x, t)\mathbf{W}_e(x, t, x', t') = \delta(x''-x')\delta(t''-t')\,\mathbf{I} \qquad (2.41)$$

$$\oint_S ds \int_0^T dt\, \mathbf{W}_g^{-1}(s'', t'', s, t)\mathbf{W}_g(s, t, s', t') = \delta(s''-s')\delta(t''-t')\,\mathbf{I} \qquad (2.42)$$

where $\mathbf{I}$ is a $J \times J$ unit matrix and J is the number of model variables.

2.5 Summary and discussion

We have shown above, following Bennett (1992), that it is straightforward to derive a formal solution to the problem of combining observations with nonlinear continuous models. It is important to realise that we have obtained a unique optimal solution to a variational assimilation problem defined by a nonlinear cost function. The derivation of the Euler–Lagrange equations explicitly uses the condition that the gradient of the cost function is zero. Furthermore, the gradient of the cost function is linear, even for the nonlinear model and observations, so that there is only one zero solution. Therefore the Euler–Lagrange equations do describe the unique optimal solution.

However, we came across the problem that the forward equations need the solution of the adjoint equations as input, while the adjoint equations require the solution of the forward equations as input. Thus the forward and adjoint equations are coupled, and together make up a boundary value problem in time. There is no straightforward solution of such problems, and several numerical approximations are needed to come to a practical numerical algorithm. Steps in this direction using the representer method have been taken by Egbert et al. (1994), Egbert and Bennett (1996), Bennett et al. (1996), and Bennett et al. (1997). We will now discuss some of the qualitative aspects of the practical solution, and refer to the above references for details (see also the appendix to this report for an introduction to representers).

First we introduce a compact notation for the observation and constraint adjoint terms,

$$\bar{\Phi}^*(\hat{\mathbf{q}}, \cdot, \cdot) = -\left(\frac{\partial \mathbf{E}}{\partial \hat{\mathbf{q}}}\right)_\cdot^* \bar{\omega}(\cdot, \cdot) + \sum_{m=1}^{M} \left(\frac{\partial H_m}{\partial \hat{\mathbf{q}}}\right)_\cdot^* [\phi_m(\cdot, \cdot)\nu_m] \qquad (2.43)$$

The dots refer to the constraints at initial and end time, on the spatial boundary, and in the interior of the model domain. For example, on the spatial boundary $\bar{\Phi}^*(\hat{\mathbf{q}}, \cdot, \cdot)$ becomes $\bar{\Phi}^*(\hat{\mathbf{q}}, \mathbf{s}, t)$ and the adjoint operator subscript is S. The complete solution can then be summarised as:

$$\bar{\lambda}(\mathbf{x}, T) = \bar{\Phi}^{*}(\hat{\mathbf{q}}, \mathbf{x}, T) \tag{2.S.1}$$

$$-\frac{\partial \bar{\lambda}(\mathbf{x}, t)}{\partial t} = \left(\frac{\partial \mathbf{F}^{0}}{\partial \hat{\mathbf{q}}}\right)_{V}^{*} \bar{\lambda}(\mathbf{x}, t) + \bar{\Phi}^{*}(\hat{\mathbf{q}}, \mathbf{x}, t) \tag{2.S.2}$$

$$-\left(\frac{\partial \mathbf{F}^{0}}{\partial \hat{\mathbf{q}}}\right)_{S}^{*} \bar{\lambda}(\mathbf{s}, t) = -\left(\frac{\partial \mathbf{G}}{\partial \hat{\mathbf{q}}}\right)_{S}^{*} \bar{\mu}(\mathbf{s}, t) + \bar{\Phi}^{*}(\hat{\mathbf{q}}, \mathbf{s}, t) \tag{2.S.3}$$

$$\mathbf{q}(\mathbf{x}, 0) = \mathbf{q}^{0}(\mathbf{x}, 0) + \int_{V} d\mathbf{x}' \, \mathbf{W}_{i}^{-1}(\mathbf{x}, \mathbf{x}')[\bar{\lambda}(\mathbf{x}', 0) + \bar{\Phi}^{*}(\hat{\mathbf{q}}, \mathbf{x}', 0)] \tag{2.S.4}$$

$$\mathbf{q}_{t} = \mathbf{F}^{0}(\mathbf{q}) + \mathbf{F}'(\mathbf{x}, t) = \int_{V} d\mathbf{x}' \int_{0}^{T} dt' \, \mathbf{W}_{f}^{-1}(\mathbf{x}, t, \mathbf{x}', t') \, \bar{\lambda}(\mathbf{x}', t') \tag{2.S.5}$$

$$\mathbf{G}(\mathbf{q}) = \mathbf{g}^{0}(\mathbf{s}, t) + \oint_{S} d\mathbf{s}' \int_{0}^{T} dt' \, \mathbf{W}_{g}^{-1}(\mathbf{s}, t, \mathbf{s}', t') \, \bar{\mu}(\mathbf{s}', t'), \quad \mathbf{s} \in S \tag{2.S.6}$$

For the sake of the following discussion, let us assume that we can solve the above equation system iteratively and that we can estimate $\bar{\Phi}^{*}$ and $\bar{\mu}$ in the Euler–Lagrange equations (2.S1–3) in terms of a previous iterate. Such a naive solution procedure will generally not converge, but it illustrates the different steps of the actual solution.

We start by integrating the adjoint variable $\bar{\lambda}$ from the given end condition and backward in time. The end condition is zero in most cases. Exceptions are when there are measurements close enough to the end time, or when the additional constraints include time derivatives, which is seldom the case. The boundary conditions for $\bar{\lambda}$ are solved as a part of the backward integration. The initial condition for the forward equation is calculated from $\bar{\lambda}$ and $\bar{\Phi}^{*}$, which are known from the adjoint integration and previous iteration, and the forward equation is integrated including a model error term that depends on the adjoint variable $\bar{\lambda}$. The boundary conditions are solved as part of the forward equations, with a boundary error $\bar{\mu}$ from previous iteration. The constraints and the observations do only appear in the adjoint equations.

We can also see what happens when we make simplifications. The adjoint equations remain unchanged, whether we assume a perfect model ($\mathbf{W}_{f}^{-1} = 0$), perfect boundary conditions ($\mathbf{W}_{g}^{-1} = 0$), or both. However the evaluation of the forward equations is less demanding with either of these assumptions, since a convolution with a covariance matrix is avoided. When both perfect model and boundaries are assumed, there is a very large change in the computational strategy, since the forward equations no longer

depend on the adjoint variables. We no longer have a coupled boundary value problem in time. An iterative solution procedure would in this case begin by solving the forward equations, and then using the forward solution in the backward integration of the adjoint equations. This is exactly what is done in four-dimensional variational assimilation.

2.6 Conclusions

In this chapter we have shown that the data assimilation problem of combining nonlinear models and observations can be solved directly without any approximations. We began by writing down a nonlinear cost function for minimizing the misfit between model, observations and other available information. Then we showed step by step how the nonlinear Euler–Lagrange (or adjoint) equations for the problem are derived. A surprising aspect of the derivation is that it is completely linear, although the involved operators are nonlinear in the model variable $\mathbf{q}$. We showed that as a consequence, the Euler–Lagrange equations describe the unique optimal solution to the variational data assimilation problem. Finally, we indicated how the forward equations and the Euler–Lagrange equations are combined to find the optimal solution.

We have included boundary conditions and any additional constraints not explicitly modelled by the forward equations in our solution by adding corresponding terms to the nonlinear costfunction. This gives rise to additional terms in the Euler–Lagrange equations.

Model errors, errors in initial and boundary conditions, as well as errors in constraints are included in the general formulation. For each of these errors, we do need error covariance matrices. The estimation of these error covariance matrices is a central part of each data assimilation system.

In summary, the general formulation given in this chapter covers most situations arising in atmospheric modelling. These results can be used in two ways. First, as a starting point for deriving a formulation of a data assimilation system for a specific model. Second, as a starting point for developing practical algorithms for data assimilation. We will apply the first of these approaches on the global shallow water equations with a tracer in the following chapter. We do plan to use some ideas from the general formulation, and some of the ideas from the appendix to this report (representers) to derive a new practical approach to data assimilation in future.

Chapter 3

The Euler–Lagrange equations for the global shallow water equations with a tracer

3.1 Introduction

We will now derive the nonlinear Euler–Lagrange equations for the global shallow water equations with a tracer using the general approach of chapter 2. These equations can then be used as the starting point for formulating particular data assimilation algorithms. Since a tracer is included in the system, we will be able to see in what ways dynamical information could possibly be derived from tracer measurements.

Some links between tracers and dynamics are obvious. Let us consider ozone in the lower stratosphere, which is mainly a passive tracer. First, ozone is transported by the wind field. If we obtain a satellite or sonde measurement of ozone that differs considerably from the modelled ozone, we could obviously change the ozone field itself. It is also possible that we could make a small change to the model wind field so that the model transports a more accurate ozone value to the measurement location. Second, we could have correlations between dynamical and ozone model errors. This knowledge could be applied to a direct construction of a better initial model field from ozone measurements. We would then make a correction to the dynamical fields in the neighbourhood (i. e. where error covariances are significant) of where measurements suggest we change the ozone field.

Once the possible links between tracer measurements and dynamics have been identified, they do need to be quantified. First steps in this direction were taken by Riishøjgaard (1996) in a simple two-dimensional model. Here we will only derive the general formulation of the problem without any quantification of the different terms. A more quantitative discussion will be a part of a future report on implementation and experimental results of a data assimilation system based on the Euler–Lagrange equations.

The Euler–Lagrange equations will be derived for a system including the curvilinear shallow water model of chapter 1, Eqs. (1.1–4). The curvilinear coordinates make the derivation longer than for a particular coordinate system, but this approach has the advantage of generality and easy applicability for different coordinate systems. This is an important point in practical applications, where several different coordinate systems have been proposed recently for solving the meteorological equations on the sphere.

3.2 Derivation of the Euler–Lagrange equations

3.2.1 The model and observations

First we rewrite the shallow water model of chapter 1 on the general form given in chapter 2. The model variables are the same as before, that is cell average momentum, perturbation height, and tracer amount,

$$\mathbf{q} = (q_1, q_2, q_3, q_4)^t = (GQ_x, GQ_y, G\Phi', G\Psi)^t \tag{3.1}$$

where G, the Jacobian of the transformation to the curvilinear coordinates, is included in the model variables. This makes the approach applicable for different coordinate systems. The equations are two-dimensional and global, so there are no boundary conditions. No additional constraints are applied on the solution. This eliminates the boundary condition and the constraints in Eqs. (2.3–4), and the remaining equations are

$$\mathbf{q}_t = \mathbf{F}^0(\mathbf{q}) + \mathbf{F}'(\mathbf{x}, t) \tag{3.2}$$

$$\mathbf{q}(\mathbf{x}, 0) = \mathbf{q}^0(\mathbf{x}, 0) + \mathbf{q}'(\mathbf{x}, 0) \tag{3.3}$$

$$\mathbf{d}(\mathbf{x}, t) = \mathbf{H}(\mathbf{q}) + \mathbf{d}'(\mathbf{x}, t) \tag{3.4}$$

For the shallow water equations the forcing term is obtained from Eq. (1.4) and Eqs. (1.9–11), i. e.

$$\mathbf{F}^0(\mathbf{q}) = \begin{bmatrix} -\nabla\cdot(\dot{\mathbf{x}}q_1) - g(G\Phi_0 + q_3)\frac{1}{h_x}\frac{\partial}{\partial x}\left(\frac{q_3}{G}\right) + \left(f + \frac{\dot{y}}{h_x}\frac{\partial h_y}{\partial x} - \frac{\dot{x}}{h_y}\frac{\partial h_x}{\partial y}\right)q_2 \\ -\nabla\cdot(\dot{\mathbf{x}}q_2) - g(G\Phi_0 + q_3)\frac{1}{h_y}\frac{\partial}{\partial y}\left(\frac{q_3}{G}\right) - \left(f + \frac{\dot{y}}{h_x}\frac{\partial h_y}{\partial x} - \frac{\dot{x}}{h_y}\frac{\partial h_x}{\partial y}\right)q_1 \\ -\nabla\cdot(\dot{\mathbf{x}}q_3) - \nabla\cdot(\dot{\mathbf{x}}G\Phi_0) \\ -\nabla\cdot(\dot{\mathbf{x}}q_4) \end{bmatrix} \tag{3.5}$$

It is convenient to use velocities in the advection and grid transformation terms of the forcing. The velocity in terms of model variables is

$$\dot{\mathbf{x}} = (\dot{x}, \dot{y})^t = \left(\frac{q_1}{h_x(G\Phi_0 + q_3)}, \frac{q_2}{h_y(G\Phi_0 + q_3)}\right)^t \tag{3.6}$$

The observations are yet to be defined, so we retain the most general formulation that covers all possible data types. The observation terms must then be further developed for each particular data type. The equations could be made simpler by not considering observations that involve time derivatives of the model variables. But we want to cover this case as well, to show the proper treatment of observations like pressure tendencies.

3.2.2 The governing Euler–Lagrange equations of the system

With the simplifications following from no boundary conditions, no constraints, and no time derivatives in the model forcing, the Euler–Lagrange equations together with the forward equations solving the above system are

$$\bar{\nu} = \mathbf{W}_d\,[\mathbf{d} - \mathbf{H}(\hat{\mathbf{q}})]' \tag{3.7}$$

$$\bar{\lambda}(\mathbf{x}, T) = \sum_{m=1}^{M} \left(\frac{\partial H_m}{\partial \hat{\mathbf{q}}}\right)_T^* [\phi_m(\mathbf{x}, T)\nu_m] \tag{3.8}$$

$$-\frac{\partial \bar{\lambda}(\mathbf{x}, t)}{\partial t} = \left(\frac{\partial \mathbf{F}^0}{\partial \hat{\mathbf{q}}}\right)_V^* \bar{\lambda}(\mathbf{x}, t) + \sum_{m=1}^{M} \left(\frac{\partial H_m}{\partial \hat{\mathbf{q}}}\right)_V^* [\phi_m(\mathbf{x}, t)\nu_m] \tag{3.9}$$

$$\hat{\mathbf{q}}(\mathbf{x}, 0) = \mathbf{q}^0(\mathbf{x}, 0) + \int_V d\mathbf{x}'\, \mathbf{W}_i^{-1}(\mathbf{x}, \mathbf{x}')\,\{\bar{\lambda}(\mathbf{x}', 0) + \sum_{m=1}^{M} \left(\frac{\partial H_m}{\partial \hat{\mathbf{q}}}\right)_0^* [\phi_m(\mathbf{x}', 0)\nu_m]\} \tag{3.10}$$

$$\hat{\mathbf{q}}_t = \mathbf{F}^0(\hat{\mathbf{q}}) + \int_V d\mathbf{x}' \int_0^T dt'\, \mathbf{W}_f^{-1}(\mathbf{x}, t, \mathbf{x}', t')\,\bar{\lambda}(\mathbf{x}', t') \tag{3.11}$$

The task that remains is to derive the functional derivatives of the model forcing and the observation operators, along with their adjoints. Observation operators will be constructed for each new observation type introduced in the model, but we will not consider them further in the present discussion.

3.2.3 The model forcing functional derivative and its adjoint

The derivation of the functional derivative of the model forcing in Eq. (3.5), and the adjoint of the functional derivative is mostly straightforward, although lengthy. The reason is that we use the model equations on conservative form, and that our model variables are the conserved quantities. In this case extra care has to be taken where the advective velocities enter the model equations, since velocity is the quota of the model variables momentum and height. The details of the derivations are in the appendix to this chapter. Here we will only illustrate the principles by an example, and then summarise the results.

As an example, consider the pressure gradient term. After obtaining the functional derivative, see Eq. (3.A.10), the adjoint follows from insertion in the gradient of the cost function. According to the definition of the adjoint, $\langle Af, g\rangle = \langle f, A^*g\rangle$, we want to replace all operations acting on the unknown vector function $\bar{\eta}$ with operations acting on the adjoint variable $\bar{\lambda}$. In particular, we use partial integrations to move derivatives between these two variables. For the pressure gradient term this gives

$$\int_0^T dt \int_V dx \left[\frac{\partial \mathbf{F}^P}{\partial \hat{\mathbf{q}}} \bar{\eta}\right]^t \bar{\lambda} = -g \int_0^T dt \int_V dx \left[G\hat{\Phi}\, \bar{\zeta}\cdot\nabla (G^{-1} \eta_3) + \eta_3\, \bar{\zeta}\cdot\nabla (G^{-1} \hat{q}_3)\right] =$$

$$= -g \int_0^T dt \left(\oint_S ds\cdot \bar{\zeta}\, \hat{\Phi}\, \eta_3 - \int_V dx\, \eta_3 \left[G^{-1} \nabla\cdot(\bar{\zeta}\, G\, \hat{\Phi}) - \bar{\zeta}\cdot\nabla (G^{-1} \hat{q}_3)\right]\right) =$$

$$= \int_0^T dt \int_V dx\, \eta_3\, g \left[G^{-1} \nabla\cdot(\bar{\zeta}\, G\, \hat{\Phi}) - \bar{\zeta}\cdot\nabla (G^{-1} \hat{q}_3)\right] = \int_0^T dt \int_V dx \left[\left(\frac{\partial \mathbf{F}^P}{\partial \hat{\mathbf{q}}}\right)^* \bar{\lambda}\right]^t \bar{\eta}$$

with notations given below in Eq. (3.14). Here we have used the divergence theorem to obtain the boundary term, which subsequently vanishes for the global shallow water equations. The functional derivative operator and its adjoint can now be compared,

$$\frac{\partial \mathbf{F}^P}{\partial \hat{\mathbf{q}}} \bar{\eta} = \begin{bmatrix} -\frac{g}{h_x}\left[G\hat{\Phi}\frac{\partial}{\partial x}\left(\frac{\eta_3}{G}\right) + \eta_3 \frac{\partial}{\partial x}\left(\frac{\hat{q}_3}{G}\right)\right] \\ -\frac{g}{h_y}\left[G\hat{\Phi}\frac{\partial}{\partial y}\left(\frac{\eta_3}{G}\right) + \eta_3 \frac{\partial}{\partial y}\left(\frac{\hat{q}_3}{G}\right)\right] \\ 0 \\ 0 \end{bmatrix} \tag{3.12}$$

$$\left(\frac{\partial \mathbf{F}^P}{\partial \hat{\mathbf{q}}}\right)^* \bar{\lambda} = \begin{bmatrix} 0 \\ 0 \\ g\left[G^{-1} \nabla\cdot(\bar{\zeta}\, G\, \hat{\Phi}) - \bar{\zeta}\cdot\nabla (G^{-1} \hat{q}_3)\right] \\ 0 \end{bmatrix} \tag{3.13}$$

The adjoint of the functional derivative of the total model forcing is given in the appendix, (3.A.13–15), and is summarised below,

$$\left(\frac{\partial \mathbf{F}^0}{\partial \hat{\mathbf{q}}}\right)^* \bar{\lambda} = \begin{bmatrix} \hat{\mathbf{x}}\cdot\nabla\, \lambda_1 + \dfrac{\hat{\mathbf{q}}_s^t}{h_x\, G\hat{\Phi}} \dfrac{\partial \bar{\lambda}}{\partial x} - (f + \hat{\theta})\, \lambda_2 - \hat{\sigma}\dfrac{\partial h_x}{\partial y} \\ \hat{\mathbf{x}}\cdot\nabla\, \lambda_2 + \dfrac{\hat{\mathbf{q}}_s^t}{h_y\, G\hat{\Phi}} \dfrac{\partial \bar{\lambda}}{\partial y} + (f + \hat{\theta})\, \lambda_1 + \hat{\sigma}\dfrac{\partial h_y}{\partial x} \\ \hat{\mathbf{x}}\cdot\nabla\, \lambda_3 - \dfrac{\hat{\mathbf{q}}_s^t (\hat{\mathbf{x}}\cdot\nabla)\bar{\lambda}}{G\hat{\Phi}} + g\left[G^{-1} \nabla\cdot(\bar{\zeta}\, G\, \hat{\Phi}) - \bar{\zeta}\cdot\nabla (G^{-1} \hat{q}_3)\right] - G\,\hat{\theta}\,\hat{\sigma} \\ \hat{\mathbf{x}}\cdot\nabla\, \lambda_4 \end{bmatrix} \tag{3.14a}$$

$$G\hat{\Phi} = G\Phi_0 + \hat{q}_3 \tag{3.14b}$$

$$\hat{\mathbf{q}}_s = (\hat{q}_1, \hat{q}_2, G\Phi_0 + \hat{q}_3, \hat{q}_4)^t \tag{3.14c}$$

$$\hat{\theta} = \frac{\hat{y}}{h_x}\frac{\partial h_y}{\partial x} - \frac{\hat{x}}{h_y}\frac{\partial h_x}{\partial y} \tag{3.14d}$$

$$\hat{\sigma} = \frac{\hat{y}\,\lambda_1}{h_x} - \frac{\hat{x}\,\lambda_2}{h_y} \tag{3.14e}$$

$$\bar{\zeta} = \left(\frac{\lambda_1}{h_x}, \frac{\lambda_2}{h_y}\right)^t \tag{3.14f}$$

3.3 Discussion

We now consider the different links between tracers and dynamics that are present in the Euler–Lagrange equations for the shallow water equations with a tracer:

a) In the *model forcing term of the Euler–Lagrange equations*, Eq. (3.14a), the tracer appears in both the momentum and height field terms (see $\hat{\mathbf{q}}_s$ and $\bar{\lambda}$). This may look surprising, since the tracer does not affect the momentum and height field in the forward equations. The explanation lies in the relationship between the forward and the Euler–Lagrange (adjoint) equations. In the forward equations, the tracer is transported by the model velocity field. The model velocity field is expressed with the model variables momentum and height. In the adjoint equations this effect is reversed, and the adjoint momentum and height variables are affected by the adjoint tracer variable. This link is present in all four-dimensional variational assimilation systems.

b) In the *observation forcing term of the Euler–Lagrange equations*, second term on the rhs of Eq. (3.9), there is a link to the dynamical variables if the tracer observation operator depends on any of the dynamical model variables. This link is certainly present in weather forecasting models whenever satellite radiances are used as observations. Then the model temperature and humidity are parts of the radiative transfer model used as observation operator for e. g. ozone. Through the Euler–Lagrange equations the ozone observations will then change both humidity and temperature, which in turn will lead to a change in the dynamical model fields.

c) In the *initial conditions of the forward equations*, Eq. (3.10), there can be a link between the tracer and dynamical fields in the correlation matrix $\mathbf{W}_i^{-1}$. These correlations are determined as a part of the scientific development of any three- and four-dimensional assimilation system. The correlation can sometimes be increased by a suitable choice of model variables or by another choice of the variables used in the data assimilation, which need not be the same as the model variables. This is an active field of research at present.

d) In the *forward model error term*, second term on the rhs of Eq. (3.11), a link between tracer and dynamics exist if their modelling errors are correlated in $\mathbf{W}_f^{-1}$. This link is not present in most assimilation systems, since they do not consider model errors explicitly. An exception is Bennett et al. (1996, 1997). If we again consider ozone, the only term that is common with the dynamics in the forward equations is the advection term. Other forcing terms in ozone are related to photochemistry and deposition and are not directly related to dynamics. If modelling of advection is inaccurate, then the modelling errors of ozone and dynamics are correlated. A correction of the ozone model error term (i. e. where there is nonzero tracer adjoint) would lead to a small correction of the dynamical model error terms as well. In weather forecast models, advection is one of the most accurately modelled processes, so this term will likely be small compared with other effects.

3.4 Conclusions

In short, the theory shows that tracer measurements can influence the dynamics of a model in four different ways: in the model forcing term of the Euler–Lagrange equations; in the observation forcing term of the Euler–Lagrange equations; in the initial conditions of the forward equations; and in the forward model error term. The relative importance of these links needs to be found out by experimentations with particular data assimilation systems and data types, and this is planned as a part of further work.

Appendix

Derivation of the adjoint of the model forcing

Consider separately the different terms of the model forcing: the advective part $\mathbf{F}^A$, the pressure gradient part $\mathbf{F}^P$, and the Coriolis and grid transformation part $\mathbf{F}^C$,

$$\mathbf{F}^0 = \mathbf{F}^A + \mathbf{F}^P + \mathbf{F}^C \tag{3.A.1}$$

The functional derivative and its adjoint are then obtained from adding the contributions from the three parts. *Since there are no boundaries and no time derivatives in the forcing for the global shallow water equations all adjoint terms associated with boundaries, initial and end conditions disappear. This is not the general case, and one should refer to chapter 2 rather than to the below equations for general rules on how the adjoints are constructed.*

The following variables will be used where applicable to simplify the notation (with $\hat{\theta}$ etc. for the optimum solution)

$$G\Phi = G\Phi_0 + q_3 \tag{3.A.2}$$

$$\mathbf{q}_s = (q_1, q_2, G\Phi, q_4)^t \tag{3.A.3}$$

$$\theta = \frac{\dot{y}}{h_x}\frac{\partial h_y}{\partial x} - \frac{\dot{x}}{h_y}\frac{\partial h_x}{\partial y} \tag{3.A.4}$$

$$\bar{\zeta} = (h_x^{-1}\lambda_1, h_y^{-1}\lambda_2)^t \tag{3.A.5}$$

$$\sigma = \frac{\dot{y}\lambda_1}{h_x} - \frac{\dot{x}\lambda_2}{h_y} \tag{3.A.6}$$

Note that $h_{1,2} = h_{x,y}$, with similar notations for position and velocity where applicable.

1) FUNCTIONAL DERIVATIVES

a) Advection terms:

$$\mathbf{F}^{A} = -\frac{\partial}{\partial x}\left(\frac{q_1 \mathbf{q}_s}{h_x G\Phi}\right) - \frac{\partial}{\partial y}\left(\frac{q_2 \mathbf{q}_s}{h_y G\Phi}\right) \tag{3.A.7}$$

$$\frac{\partial \mathbf{F}^{A}}{\partial \hat{\mathbf{q}}}\bar{\eta} = \frac{d}{d\gamma}\left\{-\frac{\partial}{\partial x}\left[\frac{(\hat{q}_1 + \gamma\eta_1)(\hat{\mathbf{q}}_s + \gamma\bar{\eta})}{h_x(G\hat{\Phi} + \gamma\eta_3)}\right] - \frac{\partial}{\partial y}\left[\frac{(\hat{q}_2 + \gamma\eta_2)(\hat{\mathbf{q}}_s + \gamma\bar{\eta})}{h_y(G\hat{\Phi} + \gamma\eta_3)}\right]\right\}_{\gamma=0} =$$

$$= -\nabla\cdot(\hat{\mathbf{x}}\bar{\eta}) - \frac{\partial}{\partial x}\left(\frac{\hat{\mathbf{q}}_s \eta_1}{h_x G\hat{\Phi}}\right) - \frac{\partial}{\partial y}\left(\frac{\hat{\mathbf{q}}_s \eta_2}{h_y G\hat{\Phi}}\right) + \nabla\cdot\left(\frac{\hat{\mathbf{x}}\hat{\mathbf{q}}_s \eta_3}{G\hat{\Phi}}\right) \tag{3.A.8}$$

b) Pressure gradient terms:

$$F^{P}_{1,2} = -\frac{gG\Phi}{h_{1,2}}\frac{\partial}{\partial x_{1,2}}\left(\frac{q_3}{G}\right) \tag{3.A.9}$$

$$\left[\frac{\partial \mathbf{F}^{P}}{\partial \hat{\mathbf{q}}}\bar{\eta}\right]_{1,2} = \frac{d}{d\gamma}\left\{-\frac{g}{h_{1,2}}(G\hat{\Phi} + \gamma\eta_3)\frac{\partial}{\partial x_{1,2}}\left(\frac{\hat{q}_3 + \gamma\eta_3}{G}\right)\right\}_{\gamma=0} =$$

$$= -\frac{g}{h_{1,2}}\left[G\hat{\Phi}\frac{\partial}{\partial x_{1,2}}\left(\frac{\eta_3}{G}\right) + \eta_3\frac{\partial}{\partial x_{1,2}}\left(\frac{\hat{q}_3}{G}\right)\right] \tag{3.A.10}$$

c) Coriolis and grid transformation terms:

$$F^{C}_{1,2} = \pm\left[f + \frac{1}{G}\frac{\partial h_y}{\partial x}\frac{q_2}{G\Phi} - \frac{1}{G}\frac{\partial h_x}{\partial y}\frac{q_1}{G\Phi}\right]q_{2,1} \tag{3.A.11}$$

$$\left[\frac{\partial \mathbf{F}^{C}}{\partial \hat{\mathbf{q}}}\bar{\eta}\right]_{1,2} = \frac{d}{d\gamma}\left\{\pm\left[f + \frac{1}{G}\frac{\partial h_y}{\partial x}\left(\frac{\hat{q}_2 + \gamma\eta_2}{G\hat{\Phi} + \gamma\eta_3}\right) - \frac{1}{G}\frac{\partial h_x}{\partial y}\left(\frac{\hat{q}_1 + \gamma\eta_1}{G\hat{\Phi} + \gamma\eta_3}\right)\right](\hat{q}_{2,1} + \gamma\eta_{2,1})\right\}_{\gamma=0} =$$

$$= \pm\left[(f + \hat{\theta})\eta_{2,1} - \frac{\partial h_x}{\partial y}\frac{\hat{x}_{2,1}}{h_{1,2}}\eta_1 + \frac{\partial h_y}{\partial x}\frac{\hat{x}_{2,1}}{h_{1,2}}\eta_2 - G\hat{\theta}\frac{\hat{x}_{2,1}}{h_{1,2}}\eta_3\right] \tag{3.A.12}$$

2) ADJOINTS

a) Advection terms:

$$\left(\frac{\partial \mathbf{F}^{\mathrm{A}}}{\partial \hat{\mathbf{q}}}\right)^{*} \bar{\lambda} = \begin{bmatrix} \hat{\dot{\mathbf{x}}} \cdot \nabla \lambda_1 + \dfrac{\hat{\mathbf{q}}_s^{\mathrm{t}}}{h_x G \hat{\Phi}} \dfrac{\partial \bar{\lambda}}{\partial x} \\ \hat{\dot{\mathbf{x}}} \cdot \nabla \lambda_2 + \dfrac{\hat{\mathbf{q}}_s^{\mathrm{t}}}{h_y G \hat{\Phi}} \dfrac{\partial \bar{\lambda}}{\partial y} \\ \hat{\dot{\mathbf{x}}} \cdot \nabla \lambda_3 - \dfrac{\hat{\mathbf{q}}_s^{\mathrm{t}} (\hat{\dot{\mathbf{x}}} \cdot \nabla) \bar{\lambda}}{G \hat{\Phi}} \\ \hat{\dot{\mathbf{x}}} \cdot \nabla \lambda_4 \end{bmatrix} \tag{3.A.13}$$

b) Pressure gradient terms:

$$\left(\frac{\partial \mathbf{F}^{\mathrm{P}}}{\partial \hat{\mathbf{q}}}\right)^{*} \bar{\lambda} = \begin{bmatrix} 0 \\ 0 \\ g\,[G^{-1} \nabla \cdot (\bar{\zeta}\, G\, \hat{\Phi}) - \bar{\zeta} \cdot \nabla\, (G^{-1} \hat{q}_3)] \\ 0 \end{bmatrix} \tag{3.A.14}$$

c) Coriolis and grid transformation terms:

$$\left(\frac{\partial \mathbf{F}^{\mathrm{C}}}{\partial \hat{\mathbf{q}}}\right)^{*} \bar{\lambda} = \begin{bmatrix} -(f + \hat{\theta})\, \lambda_2 - \hat{\sigma} \dfrac{\partial h_x}{\partial y} \\ (f + \hat{\theta})\, \lambda_1 + \hat{\sigma} \dfrac{\partial h_y}{\partial x} \\ -G\, \hat{\theta}\, \hat{\sigma} \\ 0 \end{bmatrix} \tag{3.A.15}$$

Appendix

Variational data assimilation with representers: a tutorial

A.1 Introduction

In his book *Inverse Methods in Physical Oceanography* (Bennett 1992) Bennett solves linear variational data assimilation problems via a simple approach, which consists of expanding the sought field in terms of a prior estimate calculated with the model from a first guess initial condition, and a linear combination of fields associated with the changes caused by the measurements. The latter fields are called *representers* by Bennett.

Here we will derive the representer approach to data assimilation with the help of a simple example, using a straighforward approach which simplifies some of the arguments in Bennett's book. The method applies to nonlinear problems as well. A full nonlinear integration of the model from a first guess initial condition is then combined with linearized representer equations (Bennett et al. 1996, 1997).

Keywords: variational data assimilation, weak constraint, strong constraint, Euler-Lagrange equation, adjoint.

A.2 Model and data

For demonstrating representers, a simple example is chosen, *linear wave propagation* in one dimension,

$$u_t + u_x = F_0(x, t) + F_e(x, t) \tag{A.1}$$

$$u(x, 0) = u_0(x, 0) + u_e(x, 0) \tag{A.2}$$

$$u(x, 0) = u(x, L) \tag{A.3}$$

$$d_m = u(x_m, t_m) + \varepsilon_m, \quad m = 1, 2, \ldots, M \tag{A.4}$$

where u is true wave amplitude, d are measured wave amplitudes, and F is forcing: u_t and u_x are time and space derivatives; F_0 is known forcing and F_e is model errors; u_0 is the prior estimate of the wave amplitude, calculated from first guess initial conditions, an u_e is the error in the prior estimate; and finally there are M measurements with measurement error ε_m. The field is periodic in x with period L, and the time period over which model and data are integrated will be denoted T.

An illustration of the example is given in Fig. A.1. Without forcing, the solution is a pure translation of the initial condition $u(x, 0)$ with a velocity $v = 1$, that is $u(x, t) = u(x - vt, 0)$. With forcing $u(x, t)$ changes form as well.

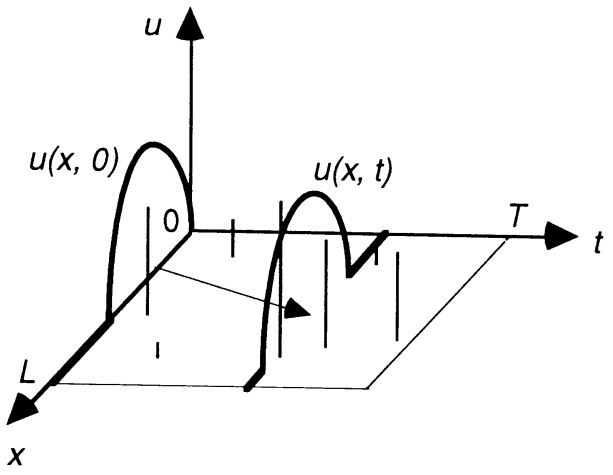

FIG. A.1: Illustration of the linear wave propagation example, Eqs. (A.1–4). Vertical lines are measurements.

F_0 could be a tidal wave component, whereas F_e could be an unknown large scale wave component.

A.3 Formulation of a variational problem to fit model and data

A solution to Eqs. (A.1–4) will be sought which minimises the following quadratic functional,

$$J[u] = W_f \int_0^L dx \int_0^T dt\,(u_t + u_x - F_0)^2 + W_i \int_0^L dx \int_0^T dt\,(u - u_0)^2 \delta(t) + W_\varepsilon \sum_{m=1}^{M} \int_0^L dx \int_0^T dt\,(d_m - u)^2\, \delta(x - x_m)\delta(t - t_m) \qquad (A.5)$$

where W_f, W_i, and W_ε are weights associated with the error in model, initial condition and data, respectively ($W \sim \sigma^{-2}$).

Constant weights imply no correlations between errors. It is straightforward to include correlations in time and space by replacing the constant weights by space and time dependent weight functions inside the integral, with no added complication except that a more elaborated notation would be used. As an example, the first integral in Eq. (A.5) would become

$$\int_0^L dx_1 \int_0^T dt_1 \int_0^L dx_2 \int_0^T dt_2\, F_e(x_1, t_1) W_f(x_1, t_1, x_2, t_2) F_e(x_2, t_2)$$

Now let the solution which gives the minimum of $J[u]$ with respect to a variation of $u(x, t)$ be $\hat{u}(x, t)$,

$$u(x, t) = \hat{u}(x, t) + \gamma\, \eta(x, t) \qquad (A.6)$$

$$\left(\frac{dJ}{d\gamma}\right)_{\gamma=0} = 0 \tag{A.7}$$

with γ a constant and $\eta(x, t)$ an arbitrary function. The interpretation of Eq. (A.6) is shown in Fig. A.2 (see Goldstein 1980 for a discussion of this standard approach to variational problems).

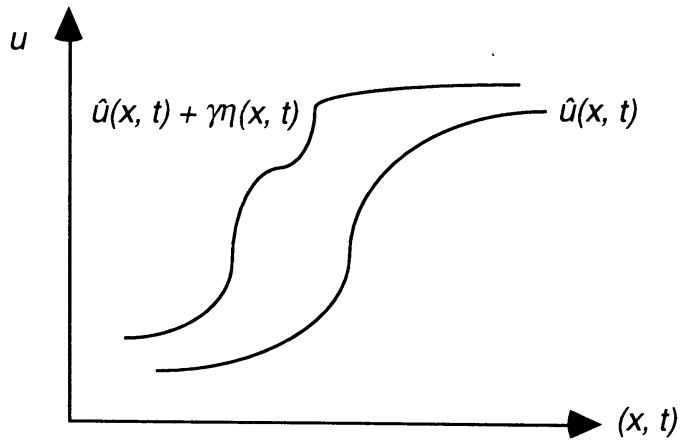

FIG. A.2: Variation of $u\,(x, t)$ to get the minimum of $J[u]$.

A.4 Solution of the variational problem

Insertion of Eqs. (A.5–6) in Eq. (A.7) gives

$$\left(\frac{dJ}{d\gamma}\right)_{\gamma=0} = \frac{d}{d\gamma}\{\int_0^L dx \int_0^T dt\,[W_f\,(\hat{u}_t + \hat{u}_x - F_0 + \gamma\eta_t + \gamma\eta_x)^2 + W_i\,(\hat{u} - u_0 + \gamma\eta)^2\delta(t)$$
$$+ W_\varepsilon \sum_{m=1}^{M} (d_m - \hat{u} - \gamma\eta)^2\,\delta(x - x_m)\delta(t - t_m)\,]\,\}_{\gamma=0} =$$
$$= 2\int_0^L dx \int_0^T dt\,[W_f\,(\hat{u}_t + \hat{u}_x - F_0)(\eta_t + \eta_x) + W_i\,(\hat{u} - u_0)\eta\,\delta(t)$$
$$- W_\varepsilon \sum_{m=1}^{M} (d_m - \hat{u})\eta\,\delta(x - x_m)\delta(t - t_m)\,] = 0$$

A standard solution is to integrate the model error term in the integral partially with respect to t and x to eliminate η_t and η_x respectively, after introducing the (adjoint) variable λ. This gives,

$$\lambda = W_f\,(\hat{u}_t + \hat{u}_x - F_0) \tag{A.8}$$

$$\int_0^L dx\,[\lambda\eta]_{t=0}^{t=T} - \int_0^L dx \int_0^T dt\,(\lambda_t + \lambda_x)\eta + \int_0^L dx \int_0^T dt\,W_i\,(\hat{u} - u_0)\eta\,\delta(t)$$
$$- \int_0^L dx \int_0^T dt\,W_\varepsilon \sum_{m=1}^{M} (d_m - \hat{u})\eta\,\delta(x - x_m)\delta(t - t_m) = 0$$

Note that an integral associated with the partial integration in x has vanished because of the periodic boundary conditions. If there were non vanishing contributions from boundary conditions, that integral would be retained without adding any problems to the solution. After rearranging terms, we get

$$\int_0^L dx\, \lambda(x, T)\eta(x, T) + \int_0^L dx\, \{W_i[\hat{u}(x, 0) - u_0(x, 0)] - \lambda(x,0)\}\eta(x, 0)$$
$$+ \int_0^L dx \int_0^T dt\, [-\lambda_t - \lambda_x - W_\varepsilon \sum_{m=1}^{M} (d_m - \hat{u})\delta(x - x_m)\delta(t - t_m)]\eta(x, t) = 0 \quad \text{(A.9)}$$

Since η is arbitrary, $\eta(x, 0)$ and $\eta(x, T)$ can be varied independently of $\eta(x, t)$, which means that the expressions in each integral must vanish. This gives the final solution, using Eqs. (A.1–2) and Eqs. (A.8–9),

$$\lambda(x, T) = 0 \quad \text{(A.10)}$$

$$-\lambda_t - \lambda_x = W_\varepsilon \sum_{m=1}^{M} (d_m - \hat{u})\delta(x - x_m)\delta(t - t_m) \quad \text{(A.11)}$$

$$\hat{u}(x, 0) = u_0(x, 0) + W_i^{-1}\lambda(x, 0) \quad \text{(A.12)}$$

$$\hat{u}_t + \hat{u}_x = F_0(x, t) + W_f^{-1}\lambda(x, t) \quad \text{(A.13)}$$

The general solution in Eqs. (A.10–13) includes an estimate of the errors in the model physics, $W_f^{-1}\lambda(x, t)$. An inverse problem of this form, where the model is not assumed to be exact, is called a *weak constraint* problem. To solve the weak constraint problem with the above formulation, $\lambda(x, t)$ must be calculated before $\hat{u}(x, t)$ can be found. Note that Eq. (A.11), derived through the variational approach, is the so called Euler-Lagrange equation for the problem.

A simplification is to assume the model to be exact, $W_f^{-1} = 0$, which gives a *strong constraint* problem. Now λ only influences $\hat{u}(x, t)$ through the initial condition. Although we still have to calculate λ, we only need to save $\lambda(x, 0)$ for the calculation of $\hat{u}(x, t)$, compared with saving the whole field $\lambda(x, t)$ when model errors are included.

We will generally need an iterative approach to solve the weak as well as strong constraint problem. First Eqs. (A.12–13) are integrated forwards in time from the first guess initial condition $u_0(x, 0)$ with $\lambda(x, t) = 0$. This gives $u_0(x, t)$, which can be used as a first estimate of $\hat{u}(x, t)$ in the backward integration of Eqs. (A.10–11). Now there is a first estimate of $\lambda(x, t)$ to use in the forward integration of Eqs. (A.12–13), etc.

The solution for the weak constraint problem is sketched in Fig. A.3. The solution of λ gives a jump at each measurement point which translates into an discontinuity in the time derivative of $\hat{u}$.

For the strong constraint problem, the solution of λ is unchanged, but λ does not any longer contribute to the forcing of $\hat{u}$, thus the time derivative of $\hat{u}$ is continuous (as long as F_0 is continuous).

Note that when error correlations in time and space are included, the changes in λ and $\hat{u}$ go via smooth transitions.

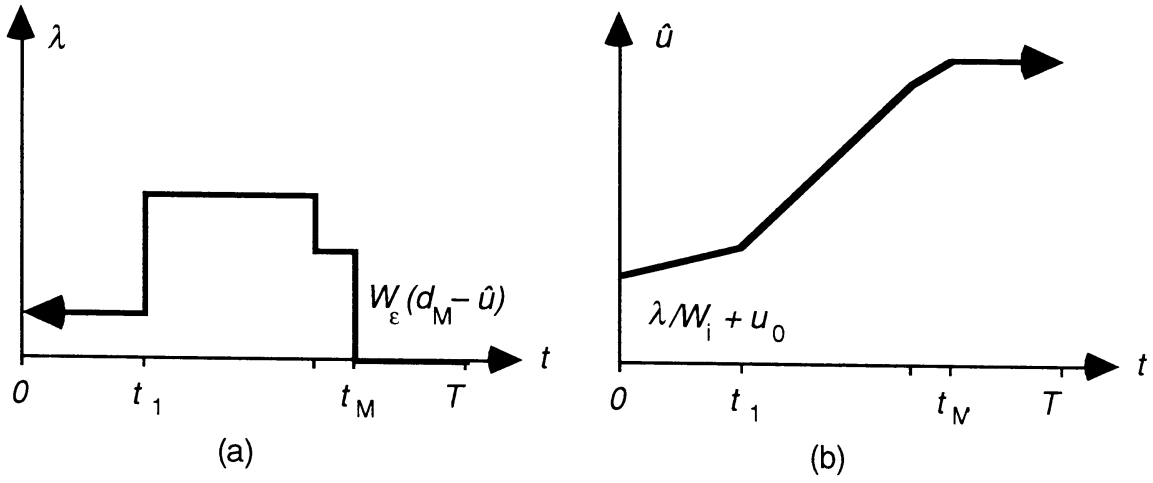

FIG. A.3: The solution of the general inverse problem with Eqs. (A.10–13). (a) Backward integration of the adjoint λ. (b) Forward integration of $\hat{u}$.

A.5 Substituting representers in the general solution

A.5.1 Introducing the representers

It is not necessary to solve the general inverse problem in Eqs. (A.10–13) iteratively. It is possible to decouple the system into a series of initial value problems. This will be achieved by introducing *representers*. The solution can always be written as a sum of the prior estimate and a remainder,

$$\hat{u}(x, t) = u_0(x, t) + \sum_{m=1}^{\infty} b_m r_m (x, t) \tag{A.14}$$

where r_m are members of some complete family of basis functions. The special basis functions which will decouple Eqs. (A.10–13) will be called representers. As will become clear later the number of coefficients b_m which can be uniquely determined equals the number of measurements M. For convenience, introduce the vector notation,

$$\hat{u}(x, t) = u_0(x, t) + \mathbf{b}^t \mathbf{r} (x, t) \tag{A.15}$$

where $\mathbf{b}$ is a coefficient vector with elements b_m, $\mathbf{b}^t$ is its transpose, and $\mathbf{r}$ is a representer vector with elements r_m.

Inserting Eq. (A.15) in Eqs. (A.11–13) gives

$$u_0(x, 0) = u_0(x, 0) \tag{A.16}$$

$$(u_0)_t + (u_0)_x = F_0(x, t) \tag{A.17}$$

$$\lambda(x, T) = 0 \tag{A.18}$$

$$-\lambda_t - \lambda_x = W_\varepsilon \sum_{m=1}^{M} (d_m - u_0 - \mathbf{b}^t \mathbf{r})\delta(x - x_m)\delta(t - t_m) \tag{A.19}$$

$$\mathbf{b}^t \mathbf{r}(x, 0) = W_i^{-1} \lambda(x, 0) \tag{A.20}$$

$$\mathbf{b}^t (\mathbf{r}_t + \mathbf{r}_x) = W_f^{-1} \lambda(x, t) \tag{A.21}$$

A.5.2 Decoupling the representer equations

The integration of the different components of the representer vector $\mathbf{r}$ in Eqs. (A.20–21) still has not been decoupled. To achieve this, let

$$\lambda = \mathbf{b}^t \bar{\alpha} \tag{A.22}$$

(Note that since the printer does not print bold Greek letters, I write all Greek vectors as $\bar{\alpha}$ etc. instead). Using Eq. (A.22) in Eqs. (A.20–21) gives

$$\mathbf{r}(x, 0) = W_i^{-1} \bar{\alpha}(x, 0) \tag{A.23}$$

$$\mathbf{r}_t + \mathbf{r}_x = W_f^{-1} \bar{\alpha}(x, t) \tag{A.24}$$

A.5.3 Decoupling the "adjoint" representer equations

Inserting Eq. (A.22) in Eqs. (A.18–19) gives the following equations for $\bar{\alpha}$, which is the adjoint representer vector,

$$\bar{\alpha}(x, T) = 0 \tag{A.25}$$

$$\mathbf{b}^t (-\bar{\alpha}_t - \bar{\alpha}_x) = W_\varepsilon \sum_{m=1}^{M} (d_m - u_0 - \mathbf{b}^t \mathbf{r})\delta(x - x_m)\delta(t - t_m) \tag{A.26}$$

In order to decouple the integration of the components of $\bar{\alpha}$ in Eq. (A.26), first write the right hand side as a scalar product of vectors. Let

$$\bar{\delta} = [\delta(x - x_1)\delta(t - t_1), \ldots, \delta(x - x_M)\delta(t - t_M)]^t \tag{A.27}$$

$$\mathbf{d} = [d_1, \ldots, d_M]^t \tag{A.28}$$

$$\mathbf{u}_0 = [u_0(x_1, t_1), \ldots, u_0(x_M, t_M)]^t \tag{A.29}$$

$$\mathbf{R} = \begin{bmatrix} r_1(x_1, t_1) & \cdots\cdots & r_1(x_M, t_M) \\ r_2(x_1, t_1) & \cdots\cdots & r_2(x_M, t_M) \\ \vdots & \vdots & \vdots \end{bmatrix} \tag{A.30}$$

These definitions give

$$W_\varepsilon \sum_{m=1}^{M} (d_m - u_0 - \mathbf{b}^t \mathbf{r})\delta(x - x_m)\delta(t - t_m) = W_\varepsilon (\mathbf{d} - \mathbf{u}_0 - \mathbf{R}^t \mathbf{b})^t \bar{\delta} = \mathbf{c}^t \bar{\delta} \tag{A.31}$$

$$\mathbf{c} = W_\varepsilon (\mathbf{d} - \mathbf{u}_0 - \mathbf{R}^t \mathbf{b}) \tag{A.32}$$

Inserting Eq. (A.31) in Eq. (A.26) gives

$$\mathbf{b}^t (-\bar{\alpha}_t - \bar{\alpha}_x) = \mathbf{c}^t \bar{\delta} \tag{A.33}$$

Now it is obvious that by choosing the first M components of $\mathbf{b}$ equal to $\mathbf{c}$ in this equation, the components of $\bar{\alpha}$ decouple into equations with trivial right hand sides. To see exactly what happens, let $\mathbf{b}'$ and $\bar{\alpha}'$ denote the vectors containing the first M components of $\mathbf{b}$ and $\bar{\alpha}$, and denote the vectors containing the remaining elements as $\mathbf{b}''$ and $\bar{\alpha}''$. Then Eq. (A.33) becomes

$$\mathbf{b}'^t (-\bar{\alpha}'_t - \bar{\alpha}'_x) = \mathbf{c}^t \bar{\delta} \tag{A.34}$$

$$\mathbf{b}''^t (-\bar{\alpha}''_t - \bar{\alpha}''_x) = 0 \tag{A.35}$$

The first M components of $\bar{\alpha}$ now follow from Eq. (A.34) by choosing

$$\mathbf{b}' = \mathbf{c} = W_\varepsilon (\mathbf{d} - \mathbf{u}_0 - \mathbf{R}^t \mathbf{b}) = W_\varepsilon (\mathbf{d} - \mathbf{u}_0 - \mathbf{R}'^t \mathbf{b}' + \mathbf{R}''^t \mathbf{b}'') \tag{A.36}$$

where the $M \times M$ matrix $\mathbf{R}'$ contains the first M rows of $\mathbf{R}$ (thus a function of the first M components of $\mathbf{r}$ at the measurement points) and $\mathbf{R}''$ includes the remaining rows. Thus,

$$-\bar{\alpha}'_t - \bar{\alpha}'_x = \bar{\delta} \tag{A.37}$$

From Eq. (A.35) it follows that $b''_m = 0$ or $\alpha''_m(x, t) = 0$. From Eqs. (A.23–24) it follows that $\alpha''_m(x, t) = 0 \Rightarrow r''_m(x, t) = 0$, so under all circumstances we have

$$\mathbf{R}''^t \mathbf{b}'' = 0 \tag{A.38}$$

Inserting this in Eq. (A.36) gives

$$\mathbf{b}' = W_\varepsilon (\mathbf{d} - \mathbf{u}_0 - \mathbf{R}'^{\mathrm{t}} \mathbf{b}')$$

$$\Leftrightarrow \quad (\mathbf{R}'^{\mathrm{t}} + W_\varepsilon^{-1} \mathbf{I})\, \mathbf{b}' = (\mathbf{d} - \mathbf{u}_0)$$

$$\Leftrightarrow \quad \mathbf{b}' = (\mathbf{R}'^{\mathrm{t}} + W_\varepsilon^{-1} \mathbf{I})^{-1} (\mathbf{d} - \mathbf{u}_0) \tag{A.39}$$

where $\mathbf{I}$ is a $M \times M$ unit matrix. We have now a complete solution for the first M components of $\mathbf{r}$, i. e. for $\mathbf{r}'$.

A.5.4 Discarding the "unobservable" part of the solution

Now the wave amplitude $\hat{u}$ which minimises the functional $J[u]$ follows by insertion in Eq. (A.15),

$$\hat{u}(x, t) = u_0(x, t) + u'(x, t) + u''(x, t) \tag{A.40a}$$

$$u'(x, t) = \mathbf{b}'^{\mathrm{t}} \mathbf{r}'(x, t) \tag{A.40b}$$

$$u''(x, t) = \mathbf{b}''^{\mathrm{t}} \mathbf{r}''(x, t) \tag{A.40c}$$

It follows from Eq. (A.38) that $u''(x_\mathrm{m}, t_\mathrm{m}) = 0$ at measurement points. This term thus represents the *unobservable* part of the optimal solution, and is orthogonal to the *observable* part $u'(x, t)$. To show that the unobservable part $u''(x, t) = 0$ everywhere for the optimal solution, insert Eq. (A.40) in Eq. (A.5) and use Eqs. (A.16–17) together with Eq. (A.38) to get

$$\begin{aligned} J[u] = {} & W_\mathrm{f} \int_0^L \mathrm{d}x \int_0^T \mathrm{d}t\, [(u'_\mathrm{t} + u'_\mathrm{x}) + (u''_\mathrm{t} + u''_\mathrm{x})]^2 + W_\mathrm{i} \int_0^L \mathrm{d}x \int_0^T \mathrm{d}t\, (u' + u'')^2 \delta(t) \\ & + W_\varepsilon \sum_{\mathrm{m}=1}^{M} \int_0^L \mathrm{d}x \int_0^T \mathrm{d}t\, (d_\mathrm{m} - u_0 - u')^2\, \delta(x - x_\mathrm{m})\, \delta(t - t_\mathrm{m}) \\ = {} & W_\mathrm{f} \int_0^L \mathrm{d}x \int_0^T \mathrm{d}t\, [(u'_\mathrm{t} + u'_\mathrm{x})^2 + (u''_\mathrm{t} + u''_\mathrm{x})^2 + 2(u'_\mathrm{t} + u'_\mathrm{x})\, (u''_\mathrm{t} + u''_\mathrm{x})\,] \\ & + W_\mathrm{i} \int_0^L \mathrm{d}x \int_0^T \mathrm{d}t\, [u'^2 + u''^2 + 2(u'^2 + u''^2)]\, \delta(t) \\ & + W_\varepsilon \sum_{\mathrm{m}=1}^{M} \int_0^L \mathrm{d}x \int_0^T \mathrm{d}t\, (d_\mathrm{m} - u_0 - u')^2\, \delta(x - x_\mathrm{m})\, \delta(t - t_\mathrm{m}) \end{aligned}$$

By using the orthogonality condition all terms involving products between u' and u'' vanish when integrated, which gives

$$\begin{aligned} \mathcal{J}[u] = & \int_0^L dx \int_0^T dt\, [W_f\,(u''_t + u''_x)^2 + W_i\, u''^2] \\ & + \int_0^L dx \int_0^T dt\, [W_f\,(u'_t + u'_x)^2 + W_i\, u'^2] \\ & + W_\varepsilon \sum_{m=1}^{M} \int_0^L dx \int_0^T dt\, (d_m - u_0 - u')^2\, \delta(x - x_m)\,\delta(t - t_m) \end{aligned} \tag{A.41}$$

Since the weights W_f and W_i are positive, it follows that the minimum of the functional $\mathcal{J}[u]$ is obtained for

$$u''(x, t) = 0 \tag{A.42}$$

Thus, the unobservable part must be put to zero, which finishes the solution of the general inverse problem by the representer method.

A.6 Summary of the representer solution

The solution derived in the previous section will now be summarised. All quantities will be unprimed, and refer to the quantities with a single prime in the previous section (the observable part) where relevant.

$$u_0\,(x, 0) = u_0\,(x, 0) \tag{A.43}$$

$$(u_0)_t + (u_0)_x = F_0\,(x, t) \tag{A.44}$$

$$\alpha_m\,(x, T) = 0\,, \qquad m = 1, 2, \ldots, M \tag{A.45}$$

$$-(\alpha_m)_t - (\alpha_m)_x = \delta(x - x_m)\,\delta(t - t_m)\,, \qquad m = 1, 2, \ldots, M \tag{A.46}$$

$$r_m\,(x, 0) = W_i^{-1}\,\alpha_m(x, 0)\,, \qquad m = 1, 2, \ldots, M \tag{A.47}$$

$$(r_m)_t + (r_m)_x = W_f^{-1}\,\alpha_m(x, t)\,, \qquad m = 1, 2, \ldots, M \tag{A.48}$$

$$\mathbf{R} = \begin{bmatrix} r_1\,(x_1\,, t_1) & \cdots\cdots & r_1\,(x_M\,, t_M) \\ \vdots & & \vdots \\ r_M\,(x_1\,, t_1) & \cdots\cdots & r_M\,(x_M\,, t_M) \end{bmatrix} \tag{A.49}$$

$$\mathbf{b} = (\mathbf{R}^t + W_\varepsilon^{-1}\,\mathbf{I})^{-1} \begin{bmatrix} d_1 - u_0\,(x_1\,, t_1) \\ \vdots \\ d_M - u_0\,(x_M\,, t_M) \end{bmatrix} \tag{A.50}$$

$$\hat{u}(x, t) = u_0(x, t) + \mathbf{b}^t\,\mathbf{r}(x, t) \tag{A.51}$$

A graphical illustration of the representer solution is given in Figs. A.4–5. From Eqs. (A.45–48) it is clear that each representer can be calculated

independently, and only needs data from one measurement, as shown in Fig. A.4.

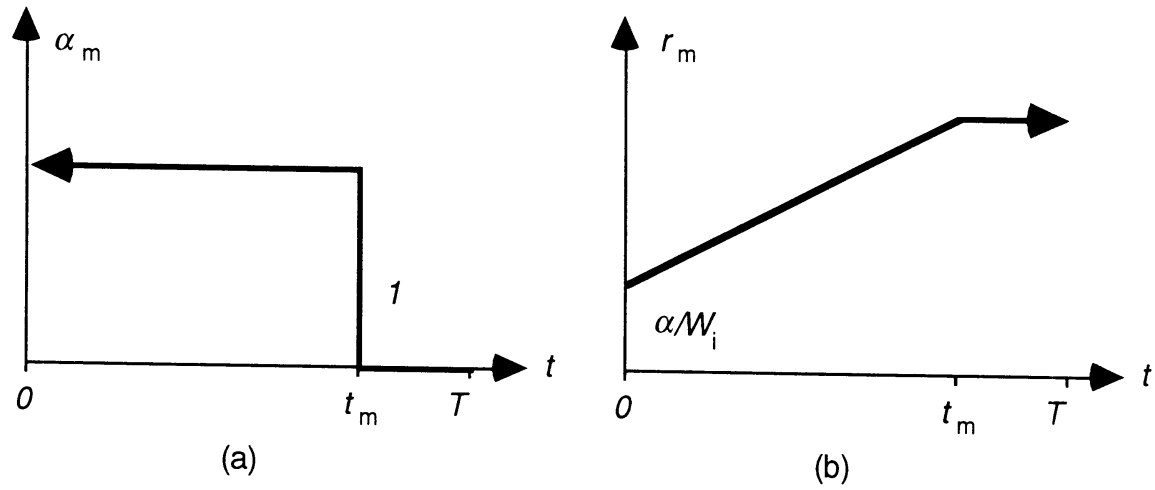

FIG. A.4: The evolution of the representer and its adjoint for one measurement, Eqs. (A.45–48). (a) Backward integration of the representer adjoint α_m. (b) Forward integration of the representer r_m.

In Fig. A.5 the whole model space is drawn to show how each representer projects the effect of one measurement onto the whole solution. Wherever the representer is nonzero, the model solution is affected by the specific measurement: the larger the amplitude of the representer, the larger the measurement influences the model solution.

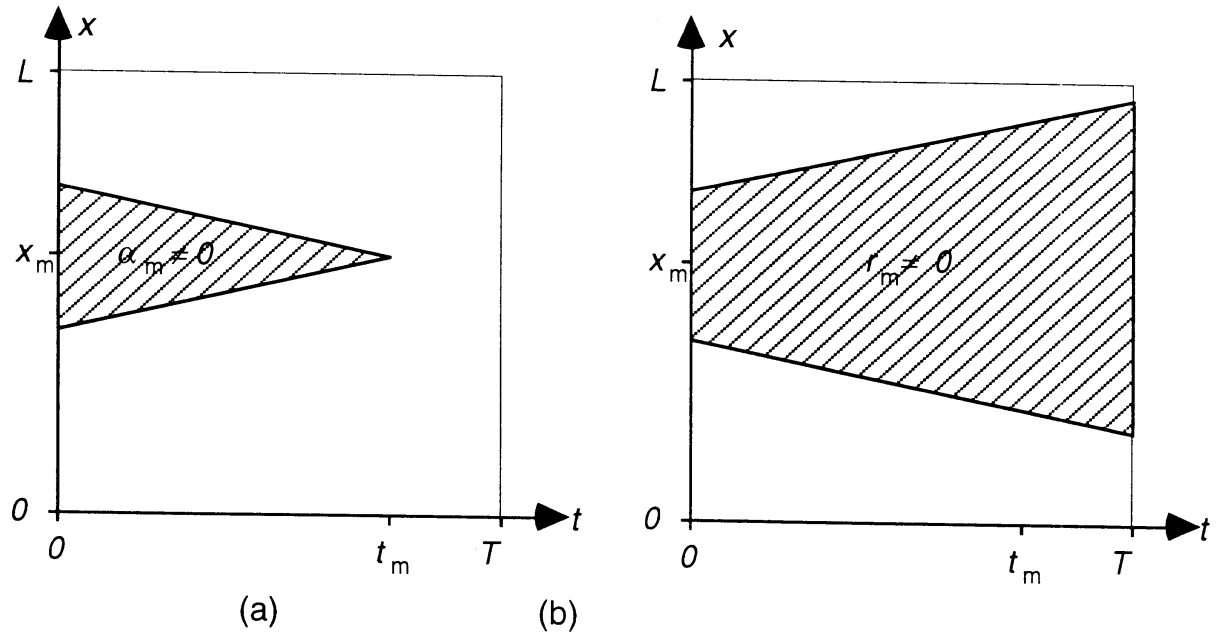

FIG. A.5: Area of influence for measurement d_m. (a) Area of influence of the representer adjoint α_m. (b) Resulting area of influence of the representer r_m.

A.7 Computational aspects of the representer solution

The calculation of the solution from Eqs. (A.43–51) are straightforward, and since each representer equation is independent, the *representers can be calculated entirely in parallel.* For *weak constraint* problems, it is necessary to save $\alpha_m(x,t)$ at all (x,t) for solving Eq. (A.48), whereas for *strong constraint* problems ($W_f^{-1} = 0$) only $\alpha_m(x,0)$ needs to be saved.

The evaluation of the final solution $\hat{u}(x,t)$ from Eq. (A.51) requires that all representers be saved at all (x,t). However, there is a trick which does not make it necessary to save $\mathbf{r}(x,t)$. From Eq. (A.36) we see that $\mathbf{b} = W_\varepsilon(\mathbf{d} - \hat{\mathbf{u}})$, using obvious notation. Thus the right hand side of Eq. (A.11) can be replace by $\mathbf{b}$. After calculating b from the representers, the representers can be discarded, and the solution $\hat{u}(x,t)$ can be calculated through Eqs. (A.10–13) whenever needed, at the cost of two model integrations and negligible extra memory requirements. These two alternative ways of calculating the optimal solution can be called the *"straightforward"* method,

$$\boxed{u_0, \bar{\alpha}, \mathbf{r}\ (2M+1 \text{ integrations}) \rightarrow \mathbf{R}, \mathbf{b} \rightarrow \hat{u} \text{ from Eq. (A.51) (large memory)}}$$

and the *"memory saving"* method which comes at the cost of two extra model integrations,

$$\boxed{u_0, \bar{\alpha}, \mathbf{r}\ (2M+1 \text{ integrations}) \rightarrow \mathbf{R}, \mathbf{b} \rightarrow \lambda\ (1 \text{ integration}) \rightarrow \hat{u}\ (1 \text{ integration})}$$

We refer to Bennett et al. (1996, 1997) for further details on efficient numerical implementation.

A.8 Final comments

We have shown by a simple example how the representer approach to variational data assimilation works. In the process the concepts of weak constraint and strong constraint problems have been explained. When applying this approach to more complicated problems, we will be faced with the formulation of the adjoint of our model. In the present case the adjoint of the model only consisted of reversing the sign in front of the derivatives, but in general the model adjoint requires much development. Another aspect is of course that in realistic problems all sorts of model and measurement error correlations enter, and here there is also considerable development needed: first, to find these correlations from measurements and model simulations; then, to implement effective ways to include the correlations in the model integration.

The representer method also opens up alternative ways to look at the data assimilation problem. Although a straightforward application of the method is not practical, there are methods to make useable representer algorithms for numerical weather prediction models as shown by Bennett et al. (1996, 1997).

References

Bennett, A. F., 1992: *Inverse methods in physical oceanography.* Cambridge University Press, 346 pp.

Bennett, A. F., B. S. Chua, and L. M. Leslie, 1996: Generalized inversion of a global numerical weather prediction model. *Meteor. Atmos. Phys.*, **60**, 165–178.

Bennett, A. F., B. S. Chua, and L. M. Leslie, 1997: Generalized inversion of a global numerical weather prediction model, II: Analysis and implementation. *Meteor. Atmos. Phys.*, **62**, 129–140.

Courtier, P. , 1997: *Dual formulation of four dimensional variational assimilation.* Submitted to Q. J. R. Meteorol. Soc.

Courtier, P. , E. Andersson, W. Heckley, J. Pailleux, D. Vasiljevic, A. Hollingsworth, F. Rabier, and M. Fisher, 1997: *The ECMWF implementation of three dimensional variational assimilation (3D–VAR). Part 1: Formulation.* Submitted to Q. J. R. Meteorol. Soc.

Daley, R., 1991: *Atmospheric Data Analysis.* Cambridge University Press, 457 pp.

Egbert, G. D., A. F. Bennett, and M. G. G. Foreman, 1994: TOPEX/POSEIDON tides estimated using a global inverse model. *J. Geophys. Res.*, **99**, 24821–24852.

Egbert, G. D., and A. F. Bennett, 1996: Data assimilation methods for ocean tides. In P. Malanotte-Rizzoli, Ed., *Modern approaches to data assimilation in ocean modelling*, Elsevier Science, Amsterdam, 147–179.

Goldstein, H., 1980: *Classical mechanics.* Second edition. Addison-Wesley Publishing Company, 672 pp.

Hólm, E. V., 1995a: A fully two-dimensional, non-oscillatory advection scheme for momentum and scalar transport equations. *Mon. Wea. Rev.*, **123**, 536–552.

Hólm, E. V., 1995b: Corrigendum. *Mon. Wea. Rev.*, **123**, 3125.

Hólm, E. V., 1996a: Energy and enstrophy conservation properties of high-order non-oscillatory advection schemes. *Tellus*, **48A**, 122–137.

Kolmogorov, A. N., and S. V. Fomin, 1957: *Elements of the theory of functions and functional analysis. Volume1: Metric and normed spaces.* Graylock Press, Rochester, 129 pp.

Levelt, P. F., M. A. F. Allaart, and H. M. Kelder, 1996: On the assimilation of total-ozone satellite data. *Ann. Geophysicae*, **14**, 1111–1118.

Lorenc, A. C., 1986: Analysis methods for numerical weather prediction. *Q. J. R. Meteorol. Soc.*, **112**, 1177–1194.

Menke, W., 1984: *Geophysical data analysis: discrete inverse theory.* Academic Press, 260 pp.

Riishøjgaard, L. P., 1996: On four-dimensional variational assimilation of ozone data in weather-prediction models. *Q. J. R. Meteorol. Soc.*, **122**, 1545–1571.

Smolarkiewicz, P. K., and L. G. Margolin, 1993: On forward-in-time differencing for fluids: Extension to a curvilinear framework. *Mon. Wea. Rev.*, **121**, 1847–1859.

Tarantola, A., 1987: *Inverse Problem Theory. Methods for data fitting and model parameter estimation*. Elsevier, Amsterdam, 613 pp.

Tarantola, A., and B. Valette, 1982: Inverse problems = Quest for information. *J. Geophys.*, **50**, 159-170.

Williamson, D. L., J. B. Drake, J. J. Hack, R. Jacob, and P. N. Swarztrauber, 1992: A standard test set for numerical approximations to the shallow water equations in spherical geometry. *J. Comput. Phys.*, **102**, 211–224.